T H E U N I V E R S I T Y O F T U L S A

THE GRADUATE SCHOOL

STUDY OF OIL/WATER EMULSION IN ELECTRIC SUBMERSIBLE PUMP – EMULSION RHEOLOGY AND ITS EFFECT ON PUMP BOOSTING PRESSURE

by
Muhammad R Ridlah

A thesis submitted in partial fulfillment of

the requirements for the degree of Master of Science

in the Discipline of Petroleum Engineering

The Graduate School

The University of Tulsa

2021

T H E U N I V E R S I T Y O F T U L S A

THE GRADUATE SCHOOL

STUDY OF OIL/WATER EMULSION IN ELECTRIC SUBMERSIBLE PUMP – EMULSION RHEOLOGY AND ITS EFFECT ON PUMP BOOSTING PRESSURE

by
Muhammad R Ridlah

A THESIS

APPROVED FOR THE DISCIPLINE OF

PETROLEUM ENGINEERING

By Thesis Committee

Hong-Quan Zhang, Chair
Ovadia Shoham
Haiwen Zhu

COPYRIGHT STATEMENT

ABSTRACT

Muhammad R. Ridlah (Master of Science in Petroleum Engineering)

Study of Oil/Water Emulsion in Electric Submersible Pump – Emulsion Rheology and Its Effect on Pump Boosting Pressure

Directed by Dr. Hong-Quan Zhang

91, pp., Chapter 5: Conclusions and Recommendations

(591 words)

Electric Submersible Pump (ESP) operation may run under up-thrust or down-thrust conditions in case of inaccurate model design thus shortening the ESP run life. The formation of tight oil/water emulsion throughout the production lifetime is inevitable and consequently induces pressure loss in the pump due to increased friction loss deteriorating the pump performance. Currently, the emulsion rheology in the ESP is still not well understood. The effective viscosity of the emulsion is commonly estimated with empirical correlations, which are only valid for a production pipeline without considering high shear in the system. This study will present the experimental investigation of emulsion rheology in the ESP along with mechanistic model development for emulsion rheology and pump hydraulic performance.

Water/oil emulsions at different water fractions and different oil viscosities are formed and circulated through a General Electric (GE) TE-2700 14-stage radial type ESP, which has 1600 specific speed (Ns), in a 3-inch closed flow loop. A pipe-in-pipe heat exchanger is installed to control the loop temperature during the experiments. Mass flow rate and fluid density are measured with the mass flowmeter. The pressure transmitters are placed over each pump stage to measure

the pressure increment. The temperature sensors are located at the pump inlet, pump outlet, and downstream of the pipe viscometer (PV). The emulsion viscosity is derived from the in-line PV downstream of the ESP discharge. The emulsion rheology and pump hydraulic performance are characterized. The comparisons of experiment results and model predictions are presented for the emulsion effective viscosity as a function of water fraction and the ESP boosting pressure at different flow rates.

Single-phase oil tests are performed at different oil viscosities and pump rotational speeds (3000 RPM, 3500 RPM) to validate the feasibility of the flow loop and pipe viscometer measurements. The PV measured viscosity shows ±6% discrepancy compared to oil viscosity from rotational viscometer measurement. Experimental results show a significant increase of emulsion viscosity at water fraction close to the inversion point due to the interactions of a great number of water droplets. The oil/water emulsion experiments are performed with two different oil viscosities, 45 cp, and 70 cp, at 3000 RPM pump speed. Higher oil viscosity reaches the inversion point at a lower water fraction. The experiment results indicate the inversion point at around 35% — 40% and 30% — 35% water-fractions, respectively.

The dimensional analysis performed by the Buckingham Pi theorem reveals that the Reynolds number, Weber number, and Strouhal number represent the combination of correction factors to the mechanistic model of emulsion viscosity. The new emulsion rheology model predictions show a good agreement with the experimental data with ±10% discrepancy. The ESP boosting pressure model begins with the Euler Equation for centrifugal pump. The mechanistic model introduces a conceptual best match flow rate (Q_{BM}) at which the outlet flow direction of the impeller matches the designed flow direction. The ESP hydraulic performance model further incorporates recirculation loss, friction loss, turn loss, and leakage loss. The increasing of water

fraction up to the inversion point deteriorates pump boosting pressure since the high friction loss occurs due to the increase of emulsion viscosity. Nevertheless, as the water fraction passes the inversion point, the boosting pressure starts to rebound with the emulsion viscosity decrease since the water changes from the dispersed phase to the continuous phase. The experiment results are compared with the mechanistic model predictions of pump hydraulic performance for oil/water emulsions with a standard deviation error less than ±20%. Additional experiment data are needed to expand the model validation for different ESP pump types and different oil viscosities.

ACKNOWLEDGEMENTS

I would like to express my deepest gratitude to Dr. Hong-Quan Zhang for his enormous trust, ideas, and supervision during the completion of this master thesis project. His encouragement and guidance have enlightened me to push my limit in finishing this project. It has been a wonderful time working in his research group, Tulsa University Artificial Lift Projects (TUALP) at the The University of Tulsa. I offer greatest gratitude to my thesis committee members: Dr. Ovadia Shoham and Dr. Haiwen Zhu for their advice, patience, and flexibility during the completion of this thesis.

I would like to thank PERTAMINA for their financial support during my study at The University of Tulsa, as well as the member companies of TUALP for their support in the completion of this project. I thank Project Engineer Mr. Bryan Sams for his help with the experiment facility, and I also thank Ms. Donna Trankley for her professional administrative assistance during my time at TUALP.

Finally, I would like to thank my beloved wife, Nadya A. Permatasari, and daughter, Aleena Rasyid, for their unconditional love and support through out the ups and downs, their belief in me goes further than my own. I thank my parents in law, and my marvelous mother, Masanah, for their endless love, prayers and limitless support. And lastly, my gratitude goes to my farther, (alm) Syafruddin, for his endeavor for the family during his lifetime, and I know that you must be proud of your son over there from heaven.

TABLE OF CONTENTS

ABSTRACT iv

ACKNOWLEDGEMENTS vii

TABLE OF CONTENTS viii

LIST OF FIGURES x

LIST OF TABLES xiii

INTRODUCTION 1

CHAPTER 1: **LITERATURE REVIEW** 4
1.1 **Alboudwarej et al** 4
1.2 **Khalil et al** 6
1.3 **Barrios et al** 7
1.4 **Emulsion Rheology Study** 9
1.4 **Croce and Pereyra** 11

CHAPTER 2: **EXPERIMENTAL SETUP** 13
2.1 **Experimental Facility** 13
2.1.1 *Experimental Flow Loop* 15
2.1.2 *Experimental ESP* 17
2.1.3 *Pipe Viscometer* 19
2.1.4 *Data Acquisition System* 20
2.2 **Experimental Program** 21
2.2.1 *Experiment Working Fluid* 21
2.2.2 *Experiment Procedure* 23
2.2.3 *Experiment Matrix* 24

CHAPTER 3: **EXPERIMENT RESULTS AND ANALYSES** 26
3.1 **Single Phase Water Experiment** 26
3.2 **Single Phase ISO-VG320 Oil Experiment** 27
3.3 **Oil/Water Emulsion Experiment** 29
3.4 **Oil/Water Emulsion Rheology** 30
3.4.1 *Pipe Viscometer (PV) Viscosity Measurement* 30
3.4.2 *Oil//Water Emulsion Rheology* 34

3.5 **Fluid Sampling** 35

CHAPTER 4: **EMULSION RHEOLOGY AND ESP PERFORMANCE MODELING** 37
4.1 **Emulsion Rheology Model** 37
4.1.1 *Model Comparison with Experiment Data* 40
4.2 **ESP Performance Model** 41
4.2.1 *Euler Equation for ESP Impeller* 42
4.2.2 *Correction Factor for Theoretical Head* 46
4.2.3 *Effective Velocity at Impeller Outlet* 47
4.2.4 *Pressure Losses* 50
4.2.4.1 Recirculation Loss 50
4.2.4.2 Friction Loss 51
4.2.4.3 Turn Loss 54
4.2.4.4 Leakage Loss 54
4.3 **Mechanistic Model Setup** 56
4.4 **Mechanistic Model Validation** 58
4.4.1 *Single Phase VG-320 Oil* 59
4.4.2 *Oil/Water Emulsion* 60
4.4.2 *Statistical Errors* 63

CHAPTER 5: **CONCLUSIONS AND RECOMMENDATIONS** 64
5.1 **Conclusions** 64
5.2.1 *Experimental Study* 64
5.2.2 *Model Development* 65
5.3 **Recommendations** 66

NOMENCLATURE 67

BIBLIOGRAPHY 73

APPENDIX A: **EQUIPMENT AND INSTRUMENT SPECIFICATIONS** 78
APPENDIX B: **DIMENSIONLESS ANALYSIS** 88
APPENDIX C: **THE STATISTICAL DEFINITION OF ERROR** 90

LIST OF FIGURES

1.1 Alboudwarej et al. Experiment Results of Emulsion Viscosities for Oil A and Oil B 5

1.2 Alboudwarej et al. Comparison between Measured and Calculated Emulsion Viscosities for Oil A and Oil B..... 6

1.3 Khalil et al. (2008) Closed Flow Loop 6

1.4 Pump Head Performance for Stable and Unstable Emulsion 7

1.5 Measured Pump Head under Different Flow Rates and Fluid Viscosities (Barrios et al. 2017) 8

1.6 HCF vs. Emulsion Viscosity for Field and Experiment Testing (Barrios et al. 2017) 9

1.7 Predicted Effective Viscosities of Water in Oil Emulsions by Selected Models… 11

1.8 Croce and Pereyra Experiment Results: (a) Effective Viscosity of Emulsion for Different Oil, (b) ISOPAR-V Oil - Pump Head at 3500 RPM, and (c) DN 20 Oil - Pump Head at 3500 RPM 12

2.1 Schematic of TUALP High-Viscosity ESP Flow Loop 13

2.2 TUALP Gas-Liquid ESP Flow Loop 14

2.3 TUALP High-Viscosity ESP Flow Loop 15

2.4 TUALP High-Viscosity ESP Flow Loop Elbow Pipe Discharge Port 15

2.5 TE-2700 ESP of TUALP High Viscosity Flow Loop 18

2.6 Catalog Pressure and Efficiency Curve from the Manufacturer 18

2.7 3D Model of TE-2700 ESP: (a) Stage Assembly, (b) Impeller, (c) Diffuser (Zhu et al. 2020) 18

2.8 Pipe Viscometer (PV) 19

2.9 Data Acquisition System of TUALP High-Viscosity ESP Flow Loop 20
2.10 Liquid Flow Rate Control of TUALP High-Viscosity ESP Flow Loop 21
2.11 Viscosity and Temperature Relationship of ISO-VG320 Oil 22
2.12 Rotational Rheometer 22
2.13 ISO-VG320 Shear Rate Tests at Different Temperatures 23
3.1 Pump Boosting Pressure Comparison with Single-Phase Water Catalog Curves 27
3.2 Experiment DP vs. Catalog Data for Single-Phase Water 27
3.3 TE-2700 ESP Performance with ISO-VG320 Oil at 3000 RPM 28
3.4 TE-2700 ESP Performance with ISO-VG320 Oil at 3500 RPM 28
3.5 TE-2700 ESP Performance with Oil/water Emulsion at 145 °F 30
3.6 TE-2700 ESP Performance with Oil/water Emulsion at 170 °F 30
3.7 Pipe Viscometer Results for Single-Phase Water Test 33
3.8 Pipe Viscometer Results for Single Phase ISO-VG320 Oil Test 33
3.9 Experiment Results of Emulsion Rheology 34
3.10 Emulsion Viscosity Measurement vs. Shear Rate at 23% Water Fraction 35
3.11 Separation Time of 32/68% W/O Emulsion Sample 36
3.12 Separation Time of 35/65% W/O Emulsion Sample 36
3.13 Separation Time of 40/60% W/O Emulsion Sample 36
4.1 Emulsion Rheology Model Compared with Experiment Data 40
4.2 Error Analysis of Emulsion Rheology Model 41
4.3 Theoretical ESP Pump Performance and Losses 42
4.4 Velocity Triangles at Impeller Inlet and Outlet 43
4.5 Velocity Triangles at Impeller Inlet and Outlet without Inlet Rotation 46

4.6 Velocity Triangles at Impeller Outlet when $Q + Q_{LK} < Q_{BM}$ 47

4.7 Recirculation Flow in Impeller 49

4.8 Velocity Triangles at Impeller Outlet when $Q + Q_{LK} > Q_{BM}$ 50

4.9 ESP Leakages through Balance Holes and Clearance (Tuzson 2000)..... 55

4.10 Leakage Geometries in an ESP Stage 55

4.11 Mechanistic Model Flow Chart 57

4.12 Tuning Mechanistic Model to Catalog Water Curve at 3000 RPM..... 58

4.13 Comparison of Mechanistic Model and Experimental Data at 3000 RPM 59

4.14 Comparison of Mechanistic Model and Experimental Data at 3500 RPM 60

4.15 Error Analysis of Mechanistic Model for Single Phase Oil 60

4.16 Comparison of Mechanistic Model and Experimental Data for Oil/Water Emulsion with 45 cp Oil Viscosity at 3000 RPM..... 61

4.17 Comparison of Mechanistic Model and Experimental Data for Oil/Water Emulsion with 70 cp Oil Viscosity at 3000 RPM..... 61

4.18 Error Analysis of Mechanistic Model for Oil/Water Emulsion with 45 cp Single Phase Oil Viscosity 62

4.19 Error Analysis of Mechanistic Model for Oil/Water Emulsion with 70 cp Single Phase Oil Viscosity 62

LIST OF TABLES

2.1 ISO-VG320 Oil Properties at Standard Condition..... 23

2.2 Experiment Test Matrix 25

4.1 Statistical Errors of Model and Data Comparisons..... 63

INTRODUCTION

Artificial lift method are introduced to optimize well performance in which the desired flow rates are higher than the natural equilibrium flow rate. The Electric Submersible Pump (ESP) transforms kinetic energy into hydraulic pressure. Thus, the ESP can help compensate for the pressure losses in the production line, including tubing, the well head, processing facilities, etc. In an ESP, a stack of centrifugal pump stages are connected by a central shaft and each pump stage has a rotational impeller and a stationary diffuser. The impeller is locked by a key to the shaft, which is rotated by a submersible motor. As a result, the liquid is accelerated by the impeller and then guided by the diffuser. The ESP has been widely used in both onshore and offshore oil fields due to its compact structure and better efficiency in high-flow-rate production compared to other artificial lift methods. Use of the ESP is not favorable for heavy oil production due to the high oil viscosity. The presence of formation water throughout the oil well production lifetime is inevitable and its volumetric rate increases as the field becomes mature. The formation water may be produced with oil in the form of an water/oil emulsion. The emulsions are stabilized by the natural surfactants or fine solids existing in the crude oil stream. The effective viscosity of the produced water/oil emulsion can rise much higher than that of the single-phase oil.

The performance of an ESP is affected by multiple factors, such as rotational speed, pump geometry, flow rates, and fluid physical properties including viscosity, density, interfacial tension, etc. In general, ESP application can be challenging because of high friction losses by the highly viscous fluid. The reduction of pump flow capacity and boosting head result in the increasing of pump brake horsepower, as well as reducing pump hydraulic efficiency correspondingly.

Oil and formation water are produced simultaneously from the reservoir to the surface. The immiscibility of those two phases (oil and water), the high rotation, and the strong shear force consequently form the dispersion and the emulsion of oil and water until the generation of a stable mixture. In most cases, the fluid phase with a lower volumetric fraction is the dispersed phase whereas the other is the continuous phase, in which the dispersed phase is distributed as droplets. Based on phase distribution, oil-water emulsions are classified into three categories: water in oil (W/O), oil in water (O/W), and complex (or multiple) mixtures. W/O and O/W are dispersions of water droplets in oil and oil droplets in water, respectively. The complex mixture (or multiple-mixture) comprises droplets that have smaller droplets of the other phase dispersed inside; both fluids are simultaneously dispersed in a continuous phase.

During the production stage, the water will increase as the field getting mature. The increase of the dispersed phase volumetric fraction will eventually lead to phase inversion, i.e., switch of the dispersed and continuous phases due to the droplets re-organization. The formation of a stable emulsion close to the inversion point results in a significant increase of effective viscosity, which dramatically reduces the ESP hydraulic performance.

The inversion points of different oils occur at different water cuts, which are important to the accurate ESP system design to ensure operational efficiency. If the ESP performance for different fluid properties is not accurately predicted, the pump may not operate around its Best Efficiency Point (BEP), thus the operation is not optimized. Presently, the industry depends on empirical correlations which were developed based on experimental data of a specific pump geometry. As a result, the correlations may not work for different pumps and their accuracy is questionable. In general, only single-phase water curves are provided by the pump manufacturers. Even performance tests are requested by customers, it is unlikely to perform experiments that cover

the variety of liquid viscosities and flow conditions. Lately, many researchers came up with the numerical simulations performed with Computational Fluid Dynamics (CFD) to study flow behavior inside ESPs. However, numerical simulations in complex flow geometries are time-consuming. In addition, the results are not reliable for oil/water emulsion since the emulsion is treated as a single-phase fluid. User-defined functions, which considers the effect of the phase interaction between continuous and dispersed phases, can be developed based on the contribution of this study to improve the ESP CFD simulation in the future.

This study presents an experimental investigation and mechanistic modeling for the emulsion rheology and its effect on ESP hydraulic performance with various oil viscosities and water fractions. The models can be used in the design and selection of the ESP system for optimum well performance. The following are the objectives of the study:

1) Acquire pump curves of single-phase liquid with different viscosities and oil/water emulsions at different water fractions. Then, analyze the pump hydraulic performance based on its boosting pressure.
2) Develop mechanitic models to predict the emulsion rheology inside the ESP and the corresponding pump boosting pressure.
3) Validate the proposed mechanistic models with measured pump curves.

Following the introduction, a literature review is summarized in Chapter 1. Details of the experimental program, the experimental facility, and the experiment results are presented in Chapter 2. The development of mechanistic models for both emulsion rheology and pump boosting pressure prediction is given in Chapter 3. The proposed new models are validated in Chapter 4. Finally, the conclusions and recommendations of this study are provided in Chapter 5.

CHAPTER 1

LITERATURE REVIEW

This chapter presents experiments and modeling studies related to oil/water emulsion characteristics under high shear environments such as centrifugal pumps and ESPs. The correlation of oil/water emulsion rheology in pump hydraulic performance is summarized.

1.1 Alboudwarej et al.

Alboudwarej et al. (2007) performed an experimental study to investigate the effect of water fraction, pressure and temperature on the heavy oil emulsion rheology. The experiment was conducted using two live heavy oil samples from South America. Live oil/water emulsions were prepared in a Taylor-Couette flow device, which is the annulus between the two concentric cylinder shear cells. The live heavy oil and synthetic formation water were set under predetermined pressure, temperature and shear condition. The emulsion stability was analyzed visually through the PVT cell. The emulsion effective viscosity was measured by a capillary viscometer.

These two working fluids were labeled as Oil A and Oil B. The experimental results indicate that viscosity is affected by temperature according to the Arrhenius relation, while the flow rate has limited effects on oil viscosity. The oil viscosity also increased linearly with the fraction of dissolved gases as the pressure decreased below the bubble point of the sample. Figure 1.1 presents the experimental results of Oil A and Oil B. The inversion point of Oil A is approximately at 50% - 55% volume water fraction, while that of Oil B at 45% - 55% water fraction.

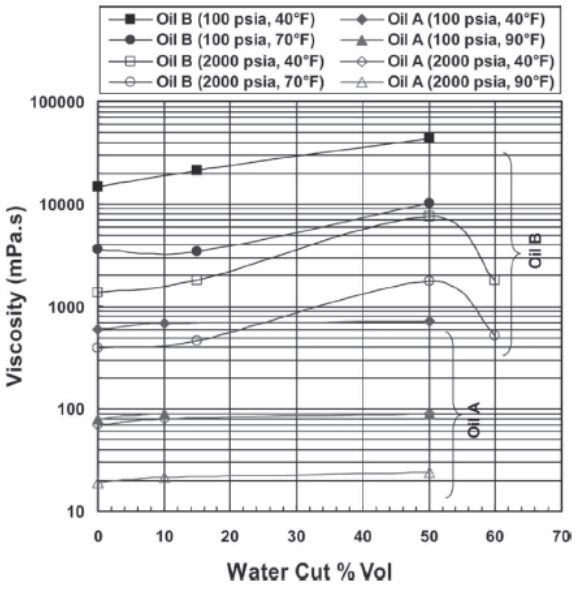

Figure 1.1: Alboudwarej et al. Experiment Results of Emulsion Viscosities for Oil A and Oil B

The study was expanded to investigate the feasibility of several well-known viscosity correlations which are available in the literature. Four single-parameter correlations were chosen for comparison. Figure 1.2 presents the comparison of measured and calculated emulsion viscosities for Oil A and Oil B. The results show that all single-parameter correlations tend to overpredict the viscosity of emulsions. Large discrepancies were observed from the plots and indicate that the correlations are largely inaccurate under high shear environment.

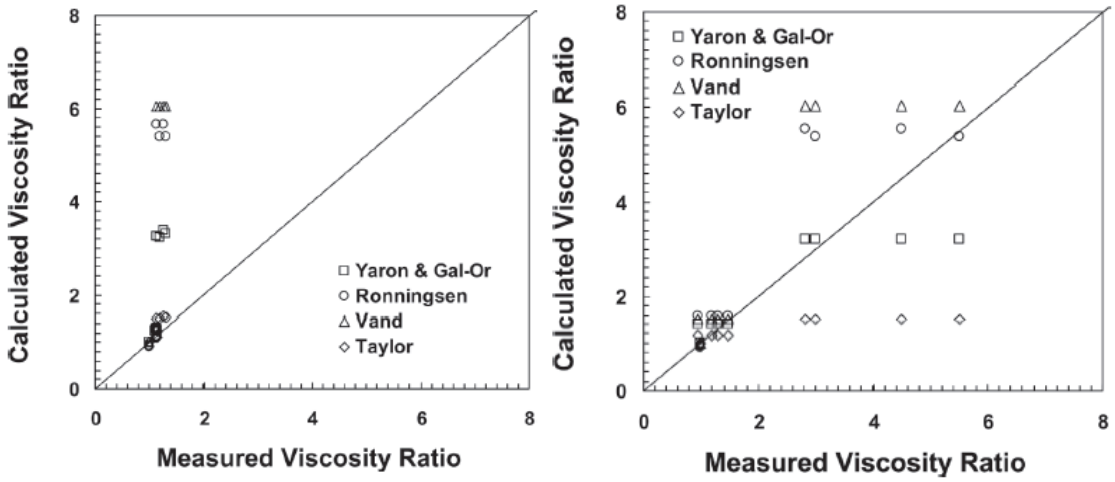

Figure 1.2: Alboudwarej et al. Comparison between Measured and Calculated Emulsion Viscosities for Oil A and Oil B

1.2 Khalil et al.

This study demonstrates the experimental investigation of centrifugal pump performance under stable and unstable oil in water emulsions at different water fractions and temperatures. The emulsions were prepared using tap water and refined white mineral oil. In one set of emulsions, the unstable emulsion was generated without a chemical emulsifier (surfactant), and the other sets were prepared with a surfactant to generate stable emulsions. As shown in Figure 1.3, the experiment facility is a closed flow loop facility that consists of motors, mixers, electric heater, centrifugal pump, pressure taps, and the choke valve. The working fluids were circulated in the flow loop and the experiment data were recorded at each specific water fraction and temperature.

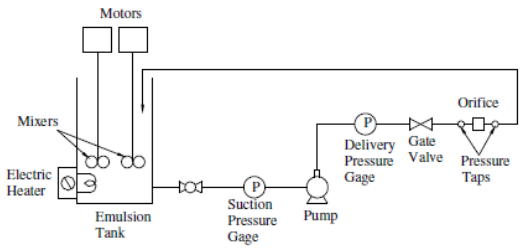

Figure 1.3: Khalil et al. (2008) Closed Flow Loop

The head-flow rate is measured at different temperatures and holdup values, and is represented by empirical relations. A comparison between head-flow curves for centrifugal pumps with water and emulsions flow is presented in Figure 1.4.

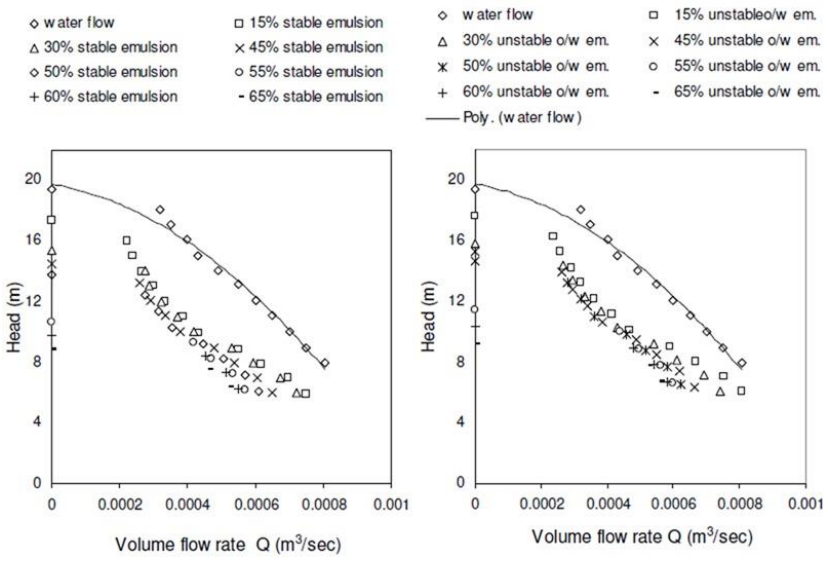

Figure 1.4: Pump Head Performance for Stable and Unstable Emulsion

In conclusion, the oil-in-water emulsion flow reduces the head and the maximum flow rate of the centrifugal pumps. As the holdup increases, the reduction in head and flow rate increases. Unstable oil-in-water emulsions show a less decrease in head-flow rate compared to stable emulsions.

1.3 Barrios et al.

Barrios et al. (2017) provided a field experience of the Caisson high power ESP technology in deepwater offshore Brazil. The study focused on the effect of high viscosity fluid due to the emulsion and the high Gas Volume Fraction (GVF). Field experience and experimental performance are compared to investigate the effect of high fluid viscosity due to emulsions. Extensive testing of the subsea boosting system was conducted at a 1500-HP ESP test land-based

facility in Houston before the construction of the Caisson ESP facility. The field pump performance was calibrated and compared with the experimental results for validation and accuracy.

The experiment results in Figure 1.5 show that as viscosity increases, the pump performance deteriorates and more horsepower is needed for the same conditions, which emphasizes the importance of a proper calculation of pump performance in the design stage to avoid production deferment.

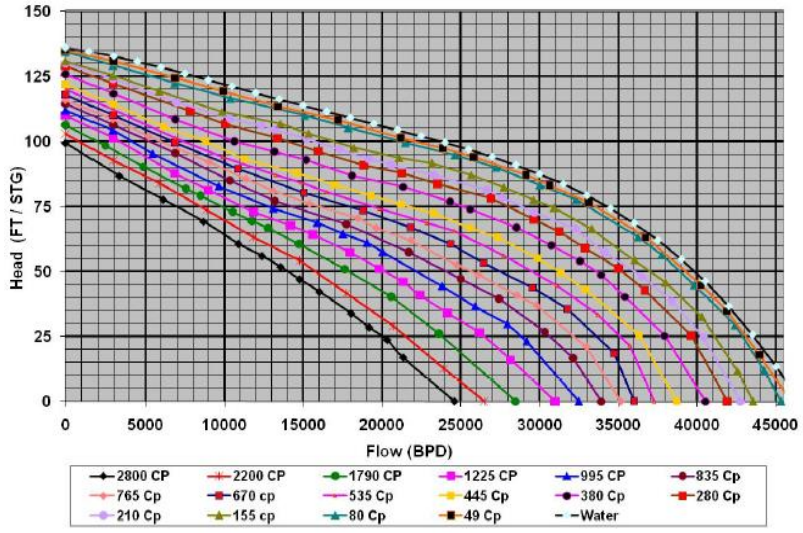

Figure 1.5: Measured Pump Head under Different Flow Rates and Fluid Viscosities (Barrios et al. 2017)

Base on the experiment results, Barrios et al. (2017) proposed the Head Correction Factor (HCF) in predicting pump performance. The Autograph PC ESP was utilized to match the head data from the experiment results. The software allows modeling of each system and calculates losses and power factors in the system, which eventually supports the selection of motor, conductor, and cable. Figure 1.6 shows the HCF for field and experiments for viscosity up to 400 cp. HCF for all viscosity is slightly higher or equal to 1 which indicates only the emulsion correction factor is required to match the pump performance.

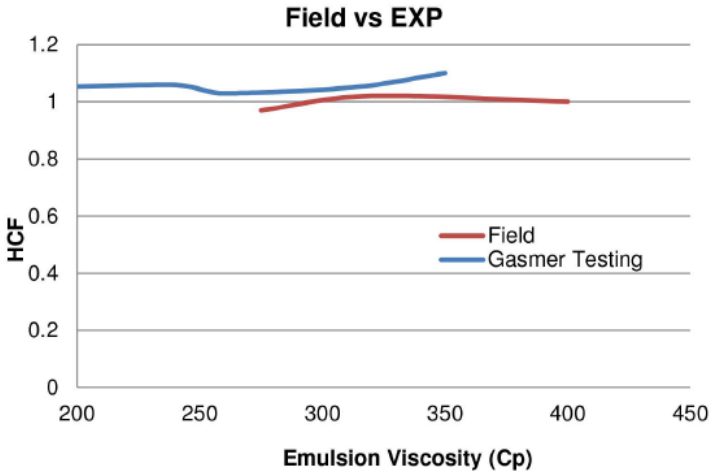

Figure 1.6: HCF vs. Emulsion Viscosity for Field and Experiment Testing (Barrios et al. 2017)

1.4 Emulsion Rheology Study

There are several studies available in the literature regarding emulsion rheology. These empirical models predict a monotonic increase of effective viscosity versus water fraction in oil continuous emulsion. All the empirical correlations are only suitable for pipe flow without considering the strong shear effect.

Einstein's (1911) relationship is based on the suspension behavior in the dilute system, and therefore it is applied up to 25% of the dispersed phase. Einstein defined the effective viscosity of emulsion as

$$\mu_m = (1 + 2.5\phi)\,\mu_o. \tag{1.1}$$

Taylor (1932) extrapolated Einstein's correlation by introducing the viscosity ratio of dispersed phase to continuous phase, which is valid for emulsions with a small dispersed spherical drop concentration:

$$\mu_m = \left(1 + 2.5\left(\frac{k+0.4}{k+1}\right)\phi\right)\,\mu_o. \tag{1.2}$$

Guth and Simha (1936) later added a quadratic term in Einstein (1911) correlation by considering the hydrodynamic interaction of two spheres, assuming spherical particles suspended in a two-immiscible-liquid mixture:

$$\mu_m = (\,1 + 2.5\phi + 14.1\phi^2)\,\mu_o. \tag{1.3}$$

Vand (1948) model considered a similar hydrodynamic interaction mechanism and arrived at an exponential relationship:

$$\mu_m = e^{\left(\frac{2.5\phi}{1-0.609\phi}\right)}\,\mu_o. \tag{1.4}$$

Brinkman (1952) extended Einstein's formula to be used with moderate particle concentrations, considering the effect of the addition of one solute molecule to an existing solution, which is treated as a continuous medium:

$$\mu_m = (\,1 - \phi\,)^{-2.5}\,\mu_o. \tag{1.5}$$

Krieger (1972) correlation considered the viscosity increase due to adding particles to a suspension already containing particles:

$$\mu_m = \left(1 - \frac{\phi}{\phi_{max}}\right)^{-2.5\phi_{max}}\,\mu_o. \tag{1.6}$$

Yaron and Gal-Or (1972) performed a rigorous analysis of the dynamic equations and derived the concentration dependent emulsion viscosity for intermediate concentrations:

$$\mu_m = \left(1 + \phi\,\frac{5.5\left[\,4\phi^{2.33} + 10 - \left(\frac{84}{11}\right)\phi^{0.75} + \left(\frac{4}{k}\right)(1-\phi^{2.33})\,\right]}{10\,(1-\phi^{3.33}) - 25\phi\,(1-\phi^{1.33}) + \left(\frac{10}{k}\right)(1-\phi)(1-\phi^{2.33})}\right)\mu_o. \tag{1.7}$$

As can be seen the above equations are formulated merely as function of the volume fraction of the water phase ϕ (i.e., water cut). In those equations, μ_m represents the mixture viscosity, μ_o represents oil viscosity, ϕ_{max} corresponds to the inversion point and k is the ratio of

the viscosity of the dispersed phase and the continuous phase. Figure 1.7. shows the calculated effective viscosities of water-in-oil emulsions vs. water cut by these rheology models.

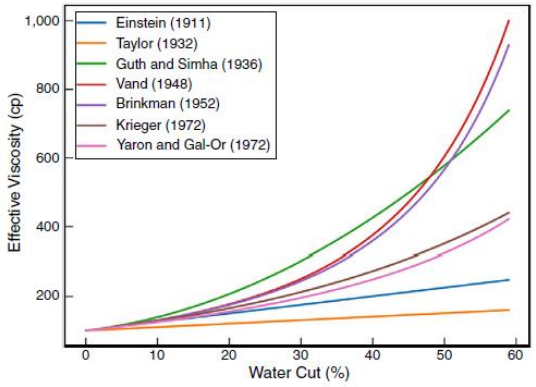

Figure 1.7: Predicted Effective Viscosities of Water in Oil Emulsions by Selected Models

1.5 Croce and Pereyra

This study presents the results of experiments conducted on a multi-stage Electric Submersible Pump (ESP) operated at constant rotating speed with two different mineral oils with viscosities of 10 cp and 125 cp, respectively. This study aimed to investigate the effect of the water fraction change on the pump performance. The effective viscosity of the emulsions was measured using a pipe viscometer set after the pump. Along with the experimental results, CFD simulations using ANSYS CFX 14.0 were carried out to understand the behavior of the phases circulated through the pump stage.

Figure 1.8 presents the experiment results of emulsion viscosity versus water fraction as well as the pump head performance for different oils with different viscosities. The effective viscosity of water in oil emulsion generated by an ESP can increase up to several times of the oil viscosity. The head delivered by the ESP is inversely proportional to the increment in emulsion viscosity.

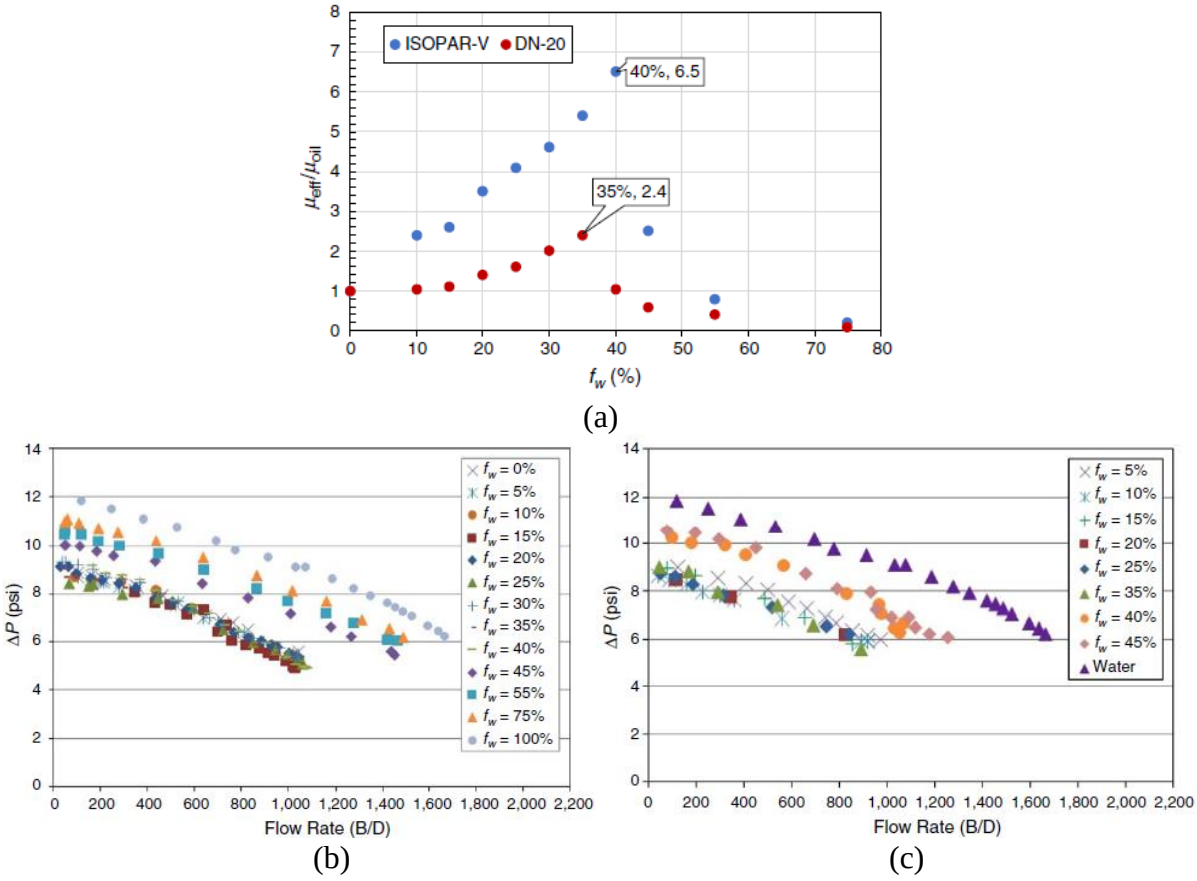

Figure 1.8: Croce and Pereyra Experiment Results: (a) Effective Viscosity of Emulsion for Different Oil, (b) ISOPAR-V Oil - Pump Head at 3500 RPM, (c) DN 20 Oil - Pump Head at 3500 RPM

CHAPTER 2

EXPERIMENTAL SETUP

The experimental facility used in this study is the same one used by Zhang (2017) to investigate the effects of high viscosity oil on the ESP performance. The objective of the current research is to extend Peng's study (2020) to investigate the oil/water emulsion rheology inside the ESP and experimentally characterize the pump hydraulic performance, and compare the experiment results with the mechanistic models.

2.1 Experimental Facility

This section provides details of the Tulsa University Artificial Lift Projects (TUALP) flow loop, instrumentation, data acquisition system, experimental programs, test matrices, as well as the testing procedure. Figure 2.1 shows the schematic of the TUALP high-viscosity ESP flow loop.

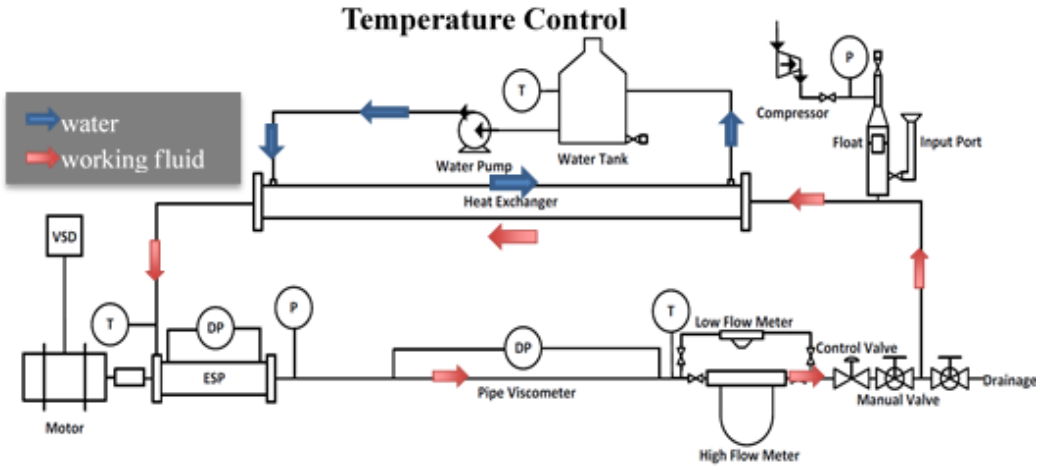

Figure 2.1: Schematic of TUALP High-Viscosity ESP Flow Loop

The experimental facility is a modification of a previous gas-liquid flow loop built by Zhu

(2017) to measure TE-2700 ESP performances under gassy conditions as shown in Figure 2.2. The pre-existing flow loop was connected to an air supply and a 150-barrel horizontal two-phase separator. The flow loop was upgraded and modified by Zhang (2017) to test TE-2700 ESP performance under high flow rate, high-viscosity fluid ranging from 1 cp to 107 cp. Later Peng (2020) tested high-viscosity fluid, ranging from 1 cp to 400 cp, and the water-in-oil emulsion flow at 5% water fraction. The original air pipeline was disconnected and the liquid flow pipe was extended to install a pipe viscometer. The modified of the TUALP high-viscosity flow loop is shown in Figure 2.3.

To discharge gas trapped inside the loop more effectively, an elbow pipe as shown in Figure 2.4 was installed to direct the gas and oil mist downward to protect students from breathing in the hazardous gas and oil mist when releasing the pressure. The flow loop has a capacity of 46.3 gallons and a maximum designed flow rate of 6,000 bpd and maximum designed pressure of 300 psig. The detailed specifications and configurations are listed in Appendix A.

Figure 2.2: TUALP Gas-Liquid ESP Flow Loop

Figure 2.3: TUALP High-Viscosity ESP Flow Loop

Figure 2.4: TUALP High-Viscosity ESP Flow Loop Elbow Pipe Discharge Port

2.1.1 Experiment Flow Loop

The existing experimental facility comprises a vertical closed flow loop with a 3-inch stainless steel pipe diameter. In this experimental study, the rotational speed of a motor (North

American H3650) is controlled by Variable Speed Drive (VSD, Hitachi L300P). The working fluids are pumped and circulated through the flow loop by TE-2700 ESP which is driven by the North American H3650 motor. In the shaft between the motor and the ESP, there is a torque sensor installed with a rotational speed sensor (Lebow 1805). The differential pressure transducers (Rosemount 3051S) are installed over each pump stage to measure the pressure increment. The pressure is monitored by an absolute pressure transmitter (Rosemount 2015) during the experiment. The wire platinum resistance temperature detectors, which are located at the ESP intake and ESP output, are installed to measure the loop temperature during the experiment. A type J thermocouple measures the fluid temperature after flowing through the pipe viscometer. The pipe viscometer consists of a hydraulic development section and a fully developed section, the pressure drop of which is measured by a differential pressure transmitter (Rosemount 3051S).

The fully developed liquid flow velocity profile can be generated after a 15-ft long hydraulic development section. Therefore, the differential pressure transmitters are placed over the 10-20 ft long fully developed section to measure the pressure drop. The pressure drop in a circular pipe is affected by fluid properties, the volumetric flow rate, and the pipe geometric parameters such as pipe diameter and length. Both mass flow rate and fluid density can be measured by two Coriolis flowmeters, one (Micro Motion CMF200) for low flow rates measurement and the other one (Proline Promass 80E) for high flow rates measurement. Two globe valves, a pneumatic valve and a manual valve, are installed to regulate the flow rates.

A compressor (Kaeser CSD60) is used to pressurize the flow loop to ensure the ESP intake pressure higher than the fluid vapor pressure to avoid cavitation. An air pressure regulator (Speedaire 4ZM22) is installed to regulate the flow loop pressure. The testing fluid is added into the loop through a transparent PVC bypass line, which indicates the loop liquid level. In the gas

discharge section, a hollow cylinder with 7.75-in length and 2.75-in diameter is submerged in the 3-inch pipe as a floater to prevent the reverse gas entrainment.

The working fluid viscosity is very sensitive to the loop temperature. Therefore, the temperature in the flow loop is maintained by a 35-ft long pipe-in-pipe heat exchanger, which is a 3-inch stainless steel pipe surrounded by the cooling water in a 6-inch PVC pipe, to transfer the heat generated by the pump. The cooling water is stored in a water tank and circulated in the 6-inch PVC pipe by a water pump (Dayton Stainless Steel Centrifugal Pump 2ZWT9A). A J thermocouple monitors the water temperature, which should be maintained to keep the viscosity of the working fluid.

2.1.2 Experimental ESP

The ESP tested in this study is a 14-stages radial type, TE-2700 with a Specific Speed (*Ns*) of 1600. The flow rate at the Best Efficiency Point (BEP) is 2700 bpd at a rotational speed of 3500 RPM. The pump manufacturer-recommended operating range at 3500 RPM is from 1500 to 3300 bpd. Figure 2.5 shows the ESP bench of the experimental facility. Except for stage 1, the differential pressure of each stage is measured. The rotational speed and pump shaft torque is measured by a torque sensor. Nevertheless, due to the increased uncertainty of the torque sensor, only part of the torque data is collected. The manufacturer water catalog curve is presented in Figure 2.6, while the flow channels of TE-2700, including impeller and diffuser, are shown in Figure 2.7.

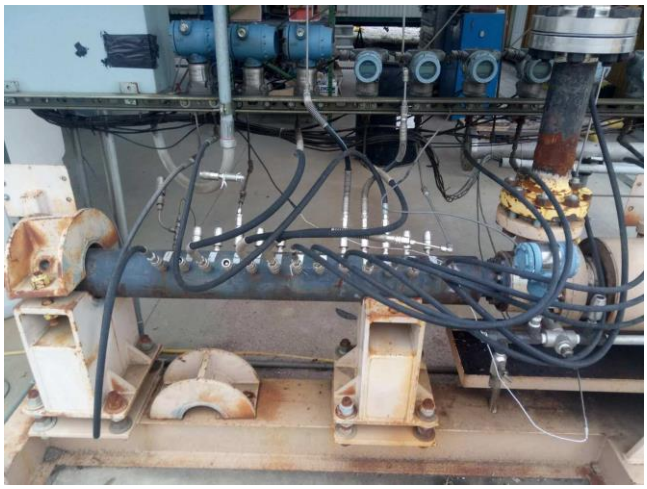

Figure 2.5: TE-2700 ESP of TUALP High-Viscosity Flow Loop

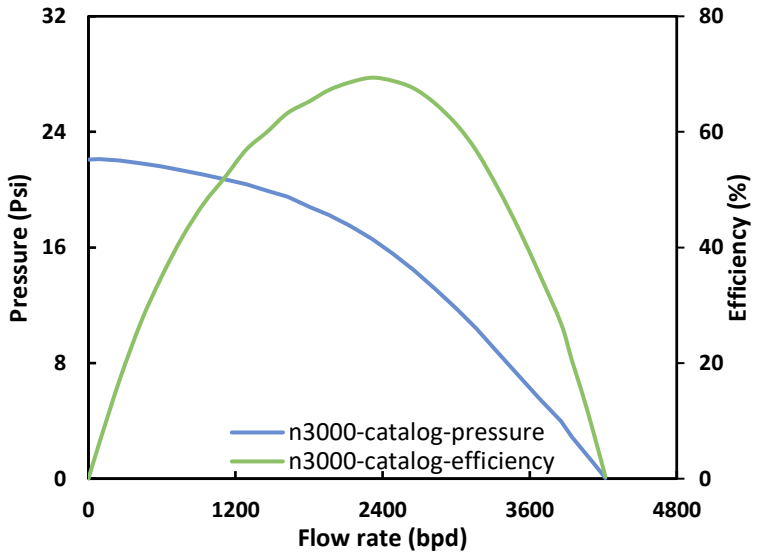

Figure 2.6: Catalog Pressure and Efficiency Curve from the Manufacturer

(a) (b) (c)

Figure 2.7: 3D Model of TE-2700 ESP: (a) Stage Assembly, (b) Impeller, (c) Diffuser (Zhu et al. 2020)

2.1.3 Pipe Viscometer

A pipe viscometer (PV) consists of a hydraulic development section and a fully developed section covered by a differential pressure transmitter. White (1998) purposed the optimum entrance length approach based on the result of a sensitivity analysis on fluid viscosity and flow rates. A 15-ft hydraulic development section is connected to the ESP outlet to allow a fully developed flow of the mixture fluid. If the dispersed phase droplet size is altered through a choke valve, the PV measured emulsion viscosity deviates from that at the ESP outlet. Therefore, the pneumatic control valve locates downstream of the PV to avoid fluid interruption that may affect the viscosity measurement. A differential pressure transmitter measures the pressure drop of the 20-ft long PV section where the flow is fully developed. Then, the fluid emulsion rheology can be calculated through pressure drop measurement.

The detailed PV geometry is shown in Figure 2.8. The recorded differential pressure can be converted into fluid effective viscosity according to the relationship between pressure loss, fluid density, volumetric flow rate, pipe diameter, pipe length, etc.,

Figure 2.8: Pipe Viscometer (PV)

2.1.4 Data Acquisition System

The instruments are connected to National Instrument (NI) modules. The output signals of pressure transmitters, temperature transmitters, and Coriolis flowmeters are transmitted to current input modules (NI cFP-AI-111). The torque sensor and the passive speed sensor are wired to a torque monitor, which transmits voltage signals to a voltage and current input module (NI cFP-AI-110). A current output module (NI cFP-AO-200) is selected to control the variable speed drive and pneumatic control valves. All NI modules are mounted on an Ethernet network interface (NI cFP-1804), which is connected to the data processing computer via an Ethernet cable.

The Data Acquisition System (DAQ) was programmed using the graphical programing language National Instrument LabVIEW V2014 in Figure 2.9. The DAQ not only serves as a monitor but also as a controller. The experiment parameters such as rotational speed, temperature, and flow rate are monitored and controlled through the LabVIEW control panel. The flow rate is controlled by adjusting the closing percentage of the pneumatic control valve in Figure 2.10, which shows the control panel display for flow rate control and adjustment. The raw data will be recorded by the DAQ and exported into a text file for data processing.

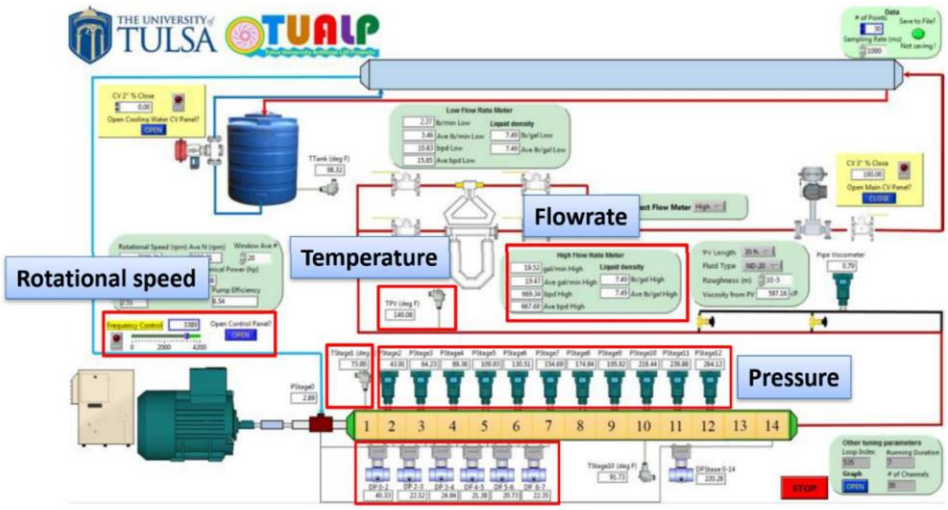

Figure 2.9: Data Acquisition System of TUALP High-Viscosity ESP Flow Loop

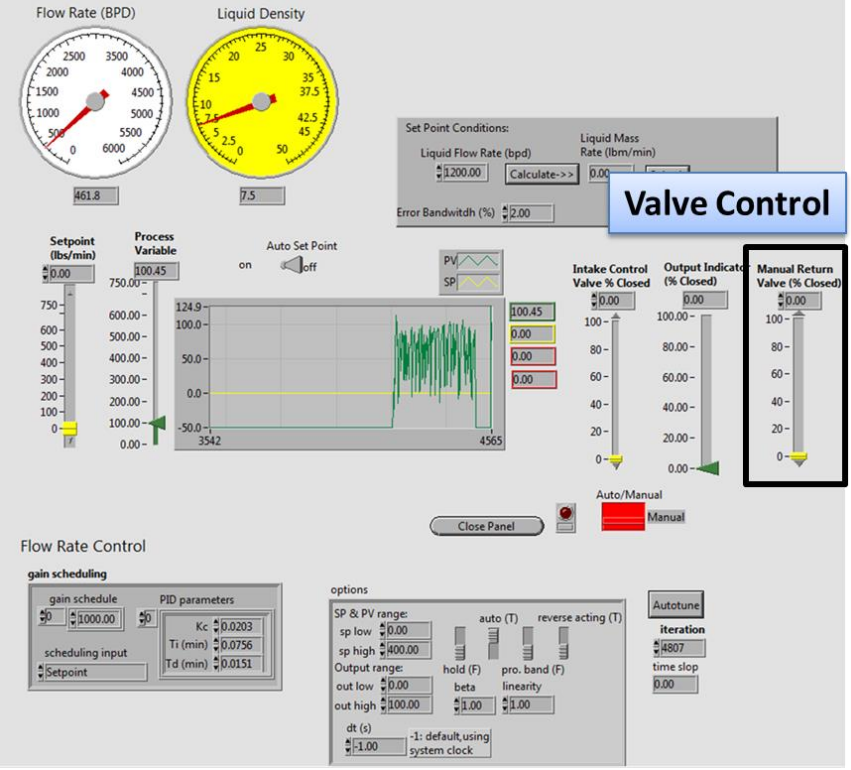

Figure 2.10: Liquid Flow Rate Control of TUALP High-Viscosity ESP Flow Loop

2.2 Experimental Program

This section provides details of the working fluid properties, the testing procedure of single-phase liquid and oil/water emulsions, and the test matrix.

2.2.1 Experiment Working Fluid

Tap water and ISO-VG320 lubricating oil are used as the working fluids in this study. Figure 2.11 shows the viscosity and temperature relationship of ISO-VG320, which was measured by the commercial rotational rheometer as shown in Figure 2.12. The viscosity of ISO-VG320 was tested at 60°F up to 175°F, and the viscosity at 60°F is 1690 cp and decreases as the temperature increases. Before the single-phase oil and emulsion testing, the flow loop was filled with tap water to test the ESP performance with water flow. As shown in Figure 2.6, the tested pump curves are compared with catalog curves to validate the accuracy of this flow loop.

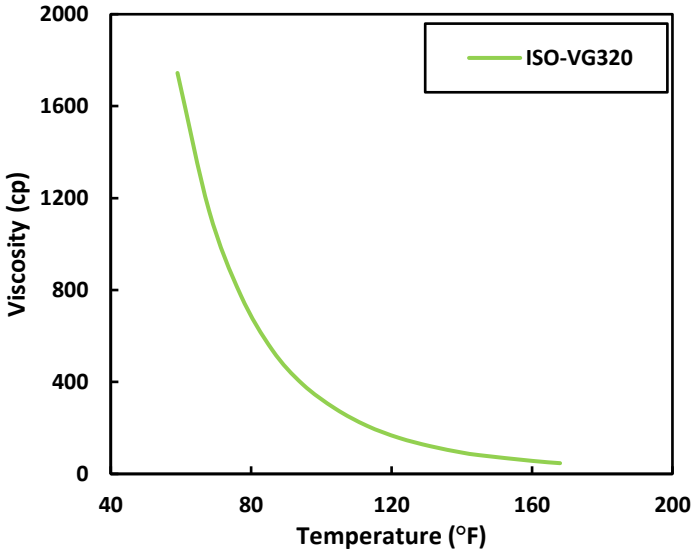

Figure 2.11: Viscosity and Temperature Relationship of ISO-VG320 Oil

Figure 2.12: Rotational Rheometer

Laboratory tests with a rotational rheometer were performed to investigate the working fluid behavior under different shear rates at three temperatures, i.e., 86°F, 104°F, and 160°F. The viscosity is independent of the shear rate as shown in Figure 2.13, which confirms the Newtonian behavior of ISO-VG320 oil.

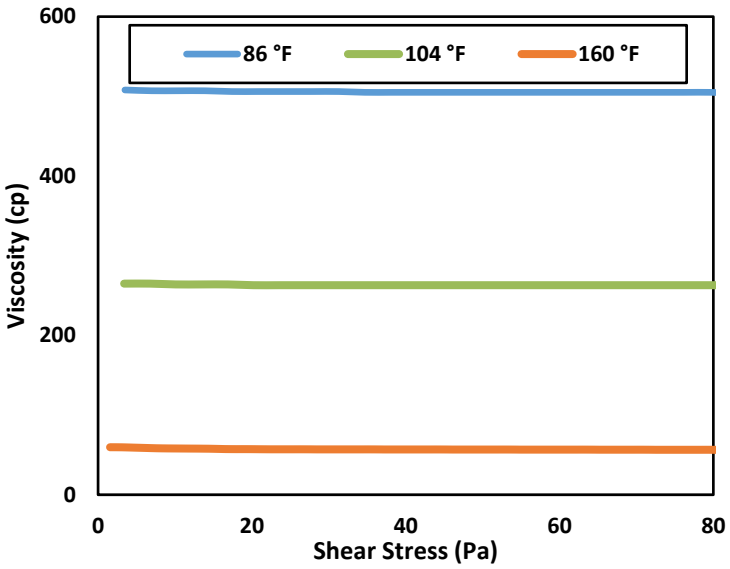

Figure 2.13: ISO-VG320 Shear Rate Tests at Different Temperatures

Tap water and lubricating oil ISO-VG320 were mixed to generate the emulsion. The mixing process was performed in the loop by running the ESP at high RPM at least for 10 minutes until the density reading is stable. The oil properties at standard conditions are shown in Table 2.1.

Table 2.1. ISO-VG320 Oil Properties at Standard Condition

Properties at SC	**ISO-VG320**	**Unit**
Density	0.86	kg/m^3
Specific Gravity	0.901	-
Viscosity	1690	cp

2.2.2 Experiment Procedure

Generally, the flow loop is first filled with the working fluid. To avoid gas being trapped in the loop, the gas release valve is opened during loop fulfillment. Then, the loop is pressurized to 30 psig to avoid pump cavitation. By running the pump at a low rotational speed, gas bubbles

trapped in the liquid are gradually separated in the discharge pipe. Then, stop the pump and the loop pressure is released to vent the gas in the discharge pipe.

The above procedure is repeated until no more gas is separated in the discharge pipe. Then, the flow loop is re-pressurized to 40 psig, and the rotational speed is increased to the designated point. The data are recorded when the temperature reaches the required value. Pump rotational speed, temperatures, pressures, differential pressures, fluid density, and flow rate are recorded every second. At each flow rate, hundred data points are collected. If the loop temperature exceeds the desired range, the pump is stopped and the loop is cooled down by the heat exchanger. The pump may need to stop multiple times until a complete pump curve is accomplished.

For the emulsion test, the experiment is performed at different water fractions. Based on the total loop volume (46.3 gallons), the water and oil volume fractions are calculated accordingly before the mixing process. A stable emulsion is formed by pump rotation after a period of high-speed operation at 60 Hz. The raw data are recorded by the DAQ and exported into the text file for further processing by a macro in Excel.

2.2.3. Experiment Matrix

The single-phase water and single-phase oil experiments were conducted at different temperatures before the water-in-oil emulsion test. Emulsions with different water and oil volume fractions were formed by mixing different amounts of tap water and lubricant ISO-VG320 oil, respectively. The test matrix is listed in Table 2.2 for all working fluids.

Table 2.2. Experiment Test Matrix

Fluid	**Water Fraction (%)**	**ESP Rotational Speed (RPM)**	**Temperature (°F)**	**Choke Opening (%)**
Tap Water	100	2400, 3000	120	100, 50, 30, 28, 26, 20, 18, 16, 14, 12, 10, 9, 8, 7, 6, 5
ISO-VG320 Oil	0	3000	140, 160, 175	
Emulsion	5, 14, 20, 23, 28, 32, 35, 40, 70, 80, 90	3000	145, 170	

CHAPTER 3

EXPERIMENT RESULTS AND ANALYSES

The experimental results for water, oil, and oil/water emulsion tests are presented and discussed in this chapter by analyzing the pump hydraulic performance and oil/water emulsion rheology.

3.1 Single-Phase Water Experiment

Prior to the oil and oil/water emulsion tests, TE-2700 ESP was tested with tap water under rotational speeds of 2400 RPM and 3000 RPM. The pump hydraulic performance is compared with the catalog curves provided by the manufacturer. Figure 3.1 presents the data comparison, in which the tested pump boosting pressure agrees well with the catalog data. The measured pump boosting pressure at low flow rates is higher than that in catalog curves, while it is lower at high flow rates. It is presumably due to the fluctuation caused by the pneumatic control valve. Overall, the data discrepancy is bounded within ±10% as shown in Figure 3.2, which validates the experiment setup of this study.

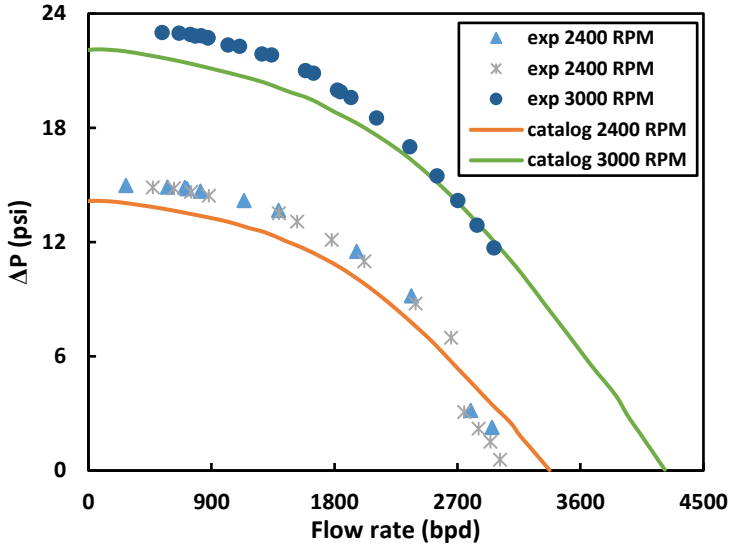

Figure 3.1: Pump Boosting Pressure Comparison with Single-Phase Water Catalog Curves

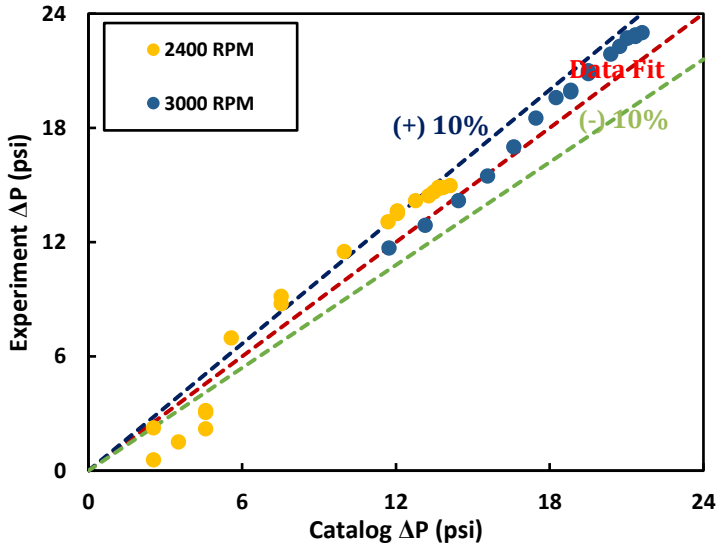

Figure 3.2: Experiment DP vs. Catalog Data for Single-Phase Water

3.2 Single-Phase ISO-VG320 Oil Experiment

The single-phase ISO-VG320 test was conducted at two pump rotational speeds 3000 RPM and 3500 RPM. The rotational rheometer (Anton Paar RheolabQC) was used to measure the oil viscosity corresponding to the testing temperature. The pump performance at 3000 RPM and 3500

RPM are presented in Figure 3.3 and Figure 3.4 separately. At both rotational speeds, the pump boosting pressure decreases as the oil viscosity increases. The increase of fluid viscosity induces higher friction loss.

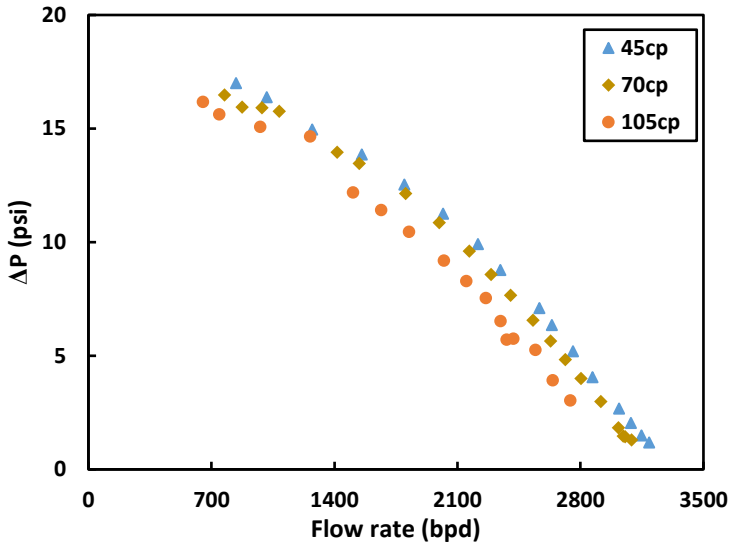

Figure 3.3: TE-2700 ESP Performance with ISO-VG320 Oil at 3000 RPM

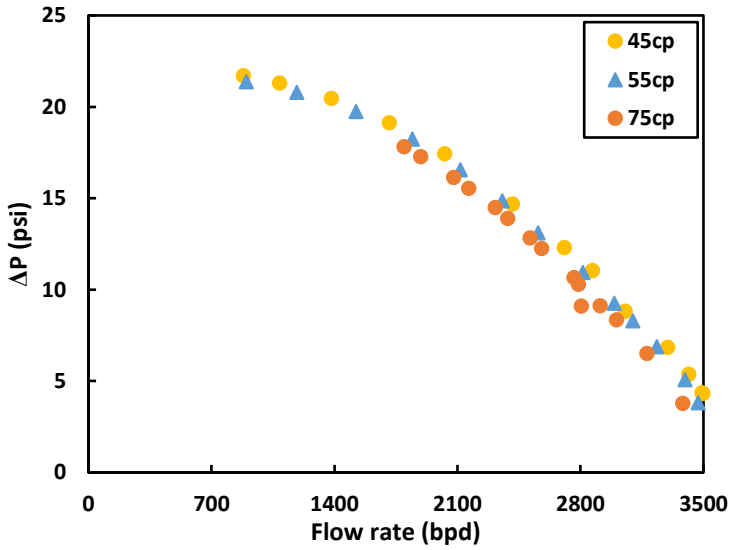

Figure 3.4: TE-2700 ESP Performance with ISO-VG320 Oil at 3500 RPM

3.3 Oil/Water Emulsion Experiment

Oil/water emulsion tests were performed at a speed of 3000 RPM. Experiments were conducted with different oil-water mixtures as listed in Table 2.2. The strong shear force acting in a rotating ESP forms dispersion and emulsion consequently. Emulsion tests were performed at different loop temperatures, i.e., 145°F and 170°F. The viscosity measurements by rotational rheometer are presented in Figure 2.11, which shows the oil viscosity is 70 cp at 145°F and 45 cp at 170°F.

It is essential to investigate the pump performance for emulsion flow versus water fraction. Figures 3.5 and 3.6 show the pump boosting pressure curves for different water fractions. Before reaching the inversion point, the emulsion viscosity increases with the increase of water fraction, which results in the degradation of ESP boosting ability. Once the water fraction exceeds the inversion point, water becomes the continuous phase and the emulsion viscosity starts to decrease sharply with the increase of water fraction. Reynolds number decreases with increase of the emulsion effective viscosity, and the pump boosting pressure curve becomes linear. Start from single-phase oil, the maximum achievable pump boosting pressure becomes lower as water fraction and emulsion effective viscosity increase. Then, the pump boosting pressure starts to increase when the water fraction is higher than 30% and 35% in Figures 3.5 and 3.6, respectively, indicating an inversion of the continuous phase. The overlap of pump curves indicates a slight change of viscosity has a limited effect on the pump performance.

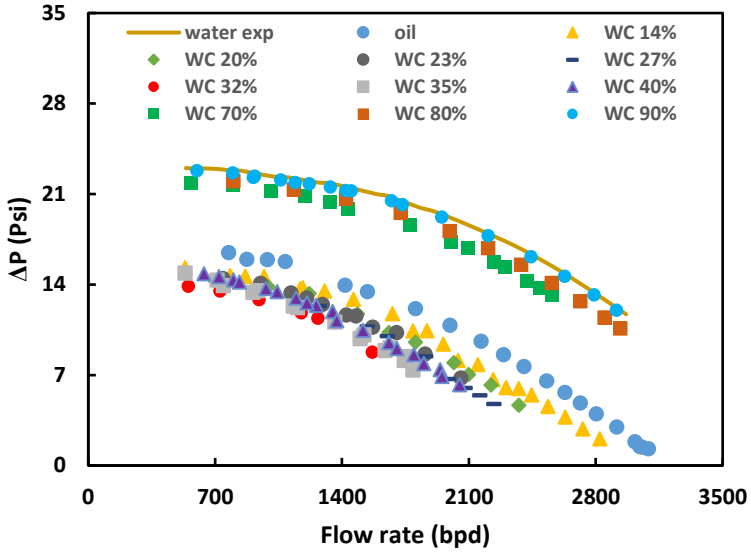

Figure 3.5: TE-2700 ESP Performance with Oil/Water Emulsions at 145°F

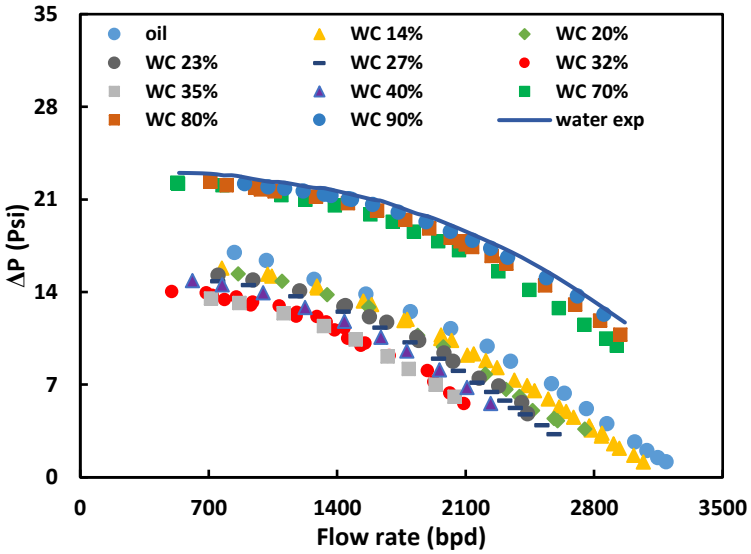

Figure 3.6: TE-2700 ESP Performance with Oil/Water Emulsions at 170°F

3.4 Oil/Water Emulsion Rheology

3.4.1. Pipe Viscometer (PV) Viscosity Measurement

The emulsion effective viscosity in experiment is derived from an in-line pipe viscometer

(PV) downstream of the ESP. Emulsion viscosity can be calculated from the flow rate and the measured pressure drop over the pipe viscometer. The calculation procedure starts from the pressure drop in pipe flow:

$$\Delta P = f\ \frac{L}{D}\ \frac{\rho V^2}{2} \tag{3.1}$$

For a high oil viscosity emulsion test, the flow regime is usually laminar if oil is the continuous phase since the Reynolds number (*Re*) is less than 2000. As a result, the Reynolds number can be related to the laminar Moody friction factor:

$$Re = \frac{64}{f}. \tag{3.2}$$

On the other hand, *Re* is defined as:

$$Re = \frac{\rho V D}{\mu}. \tag{3.3}$$

Combining Equations (3.1) to (3.3), the pressure drop in pipe flow can be expressed as:

$$\Delta P = 128 \frac{\mu L Q}{\pi D^4}. \tag{3.4}$$

Then, the viscosity can be computed as:

$$\mu = \frac{\Delta P \pi D^4}{128 L Q}, \tag{3.5}$$

which can be converted to British Unit as:

$$\mu\ (1000 \frac{cP}{Pa.s}) = \frac{\Delta P\ \left(\frac{1\ psi}{6894.76\ Pa}\right) \pi\ D^4\ (39.37 \frac{inch}{m})^4}{128\ L\ \left(3.28 \frac{ft}{m}\right) Q\ (543439.65 \frac{bpd}{m3/s})}. \tag{3.6}$$

Considering the PV geometry of this study, (3-inch pipe diameter and 20-feet length), the fluid viscosity can be expressed as:

$$\mu = 556315 \frac{\Delta P\ (psi)}{Q\ (bpd)}. \tag{3.7}$$

For a low emulsion viscosity test when water is the continuous phase, the flow is likely in the turbulent flow regime, especially at high flow rate. There are several correlations developed to calculate the turbulent pipe flow friction factor, among which the Colebrook approach (1939) in Equation (3.8) is the most popular one. The friction factor depends on not only Reynolds number, but also the relative pipe roughness (ε/D). The friction factor for turbulent flow can be calculated as:

$$\frac{1}{\sqrt{f}} = -2\log\left(\frac{\varepsilon}{3.7D} + \frac{2.51}{Re\sqrt{f}}\right). \tag{3.8}$$

Combining Equation (3.3) and Equation (3.8), the fluid viscosity for turbulent flow can be estimated as:

$$\mu = \frac{\rho VD\sqrt{f}}{2.51}\left(10^{\frac{1}{2\sqrt{f}}} - \frac{\varepsilon}{3.7D}\right). \tag{3.9}$$

Knowing the water viscosity is 1 cp, the expected differential pressure can be estimated using Equations (3.1), (3.2), (3.3), and (3.8) based on the flow regime. The comparison of experimental measurements and model predictions is shown in Figure 3.7, which shows a good agreement at low flow rates. The discrepancy increases at high flow rates, which is presumably due to the fluctuation caused by the unstable pneumatic control valve. However, the data discrepancy is still less than 10%, hence the pipe viscometer can be used to estimate the viscosity of the working fluids.

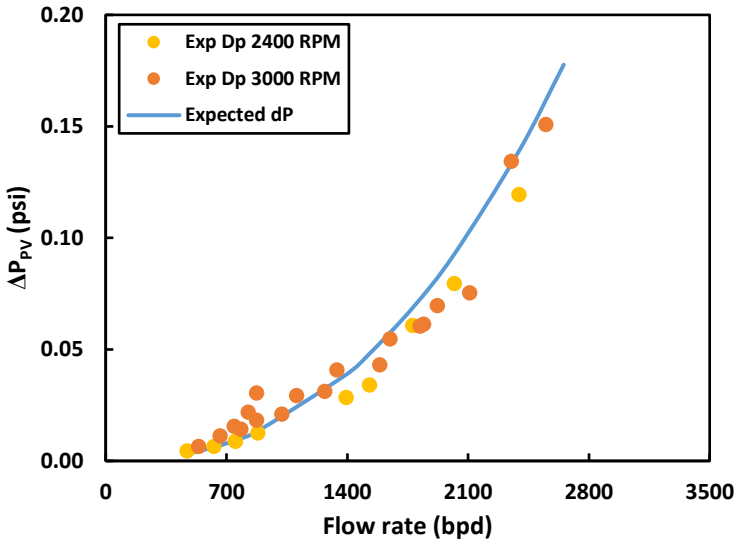

Figure 3.7: Pipe Viscometer Results for Single-Phase Water Test

The accuracy of the pipe viscometer is further tested to assure the feasibility of the experimental facility by comparing the viscosity measured by the rheometer in Figure 3.8. The discrepancy is within ±6%, which confirms the feasibility of the pipe viscometer.

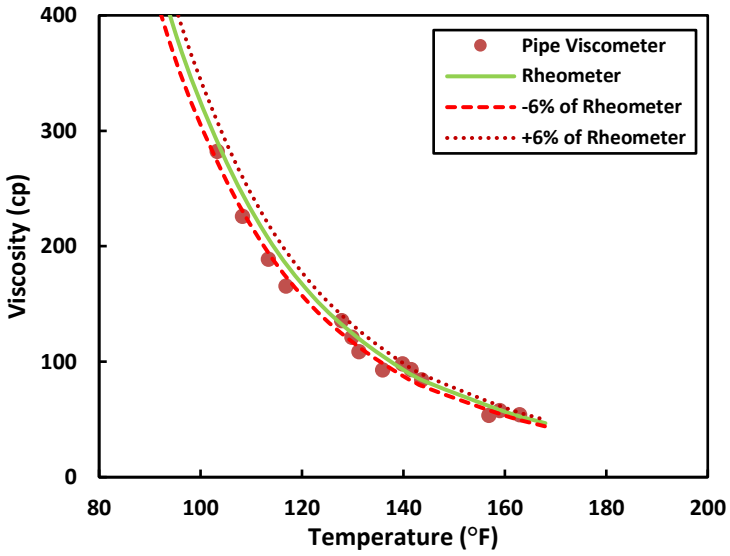

Figure 3.8: Pipe Viscometer Results for Single-Phase ISO-VG320 Oil Test

3.4.2. Oil/Water Emulsion Rheology

Emulsion tests were conducted with ISO-VG320 at different viscosities (45 cp and 70 cp), which is realized by controlling loop temperature. The relationship between emulsion viscosity and water fraction is shown in Figure 3.9. Starting from single-phase oil, the emulsion viscosity first increases with the increase of water fraction, then starts to decrease after the inversion point. This is the typical behavior of dispersed-oil/water systems, as presented in the works of Arirachakaran et al. (1989) and Vielma (2006). The emulsions behavior and continuous phase change dramatically over the inversion point. Before the inversion point, the water is the dispersed phase, and water droplets are dispersed in the oil phase, which is known as water-in-oil (W/O) emulsion. Moreover, when passing the inversion point, the oil phase starts to break down to droplets and disperses in the water. As a result, the water transforms to the continuous phase, forming oil-in-water (O/W) emulsion. As shown in Figure 3.9, the inversion point of emulsion with 45 cp oil is 35% water fraction, while that of 70 cp oil is 32% water fraction.

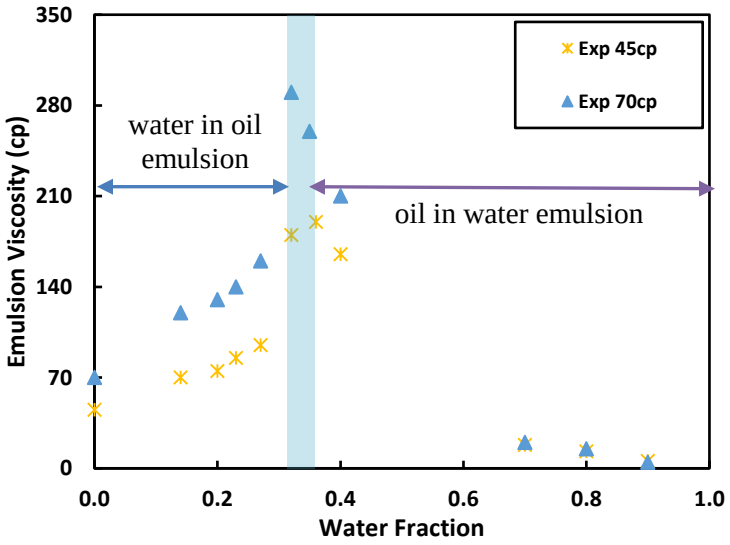

Figure 3.9: Experiment Results of Emulsion Rheology

One of the challenges in oil/water emulsion tests is its transient behavior. The emulsion

rheological properties, such as the effective viscosity and the dispersed droplet size, change with time and flow conditions. The rheology test was conducted to investigate the non-Newtonian behavior of the emulsion, i.e., emulsion effective viscosity vs. share rate. Figure 3.10 shows the viscosity measurements of the 23% water fraction emulsion, which is close to the inversion point, by rotational rheometer. The measurements were recorded at 145°F and 170°F, respectively. The results demonstrate a non-Newtonian behavior of shear thinning as shown in Figure 3.10.

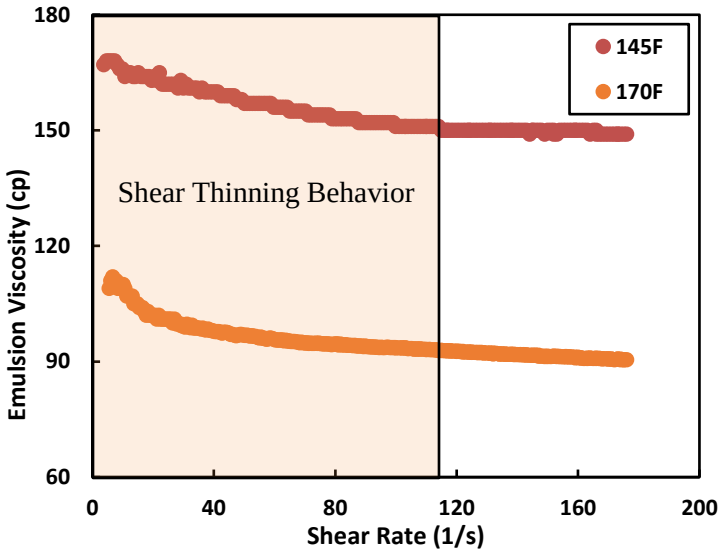

Figure 3.10: Emulsion Viscosity Measurement vs. Shear Rate at 23% Water Fraction

3.5 Fluid Sampling

ESP experiments were performed using different water and oil mixtures. The fluid samples were collected from the discharge port of the loop to observe the emulsion and dispersion stability. Beakers were used to investigate the gas entrainment and water fraction. Gas was gradually released from samples, and the volume was recorded to estimate its fraction. The oil/water emulsion samples were stored until oil and water were completely separated. Then, the water cut was calculated. Stable emulsions were formed in the test, which can be observed quantitatively

through the sampled fluids. Oil-water mixtures (32%, 35%, and 40% water fractions) at different separation times are presented in Figures 3.11, 3.12, and 3.13, respectively.

Figure 3.11: Separation Time of 32/68% W/O Emulsion Sample

Figure 3.12: Separation Time of 35/65% W/O Emulsion Sample

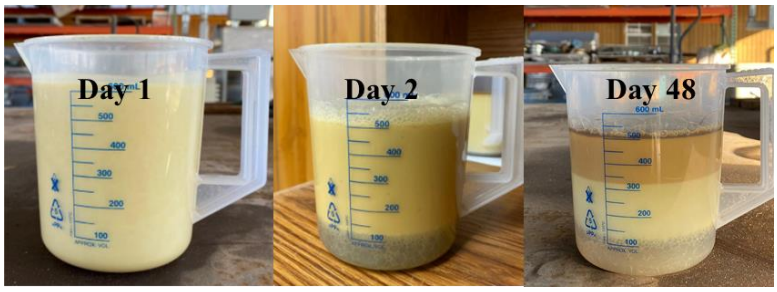

Figure 3.13: Separation Time of 40/60% W/O Emulsion Sample

It took hours and even days to separate water from the mixture. Therefore, the mixture can be classified as a stable emulsion. The layering time is faster when the water fraction is over the inversion point (water continuous) as shown in Figure 3.13. On the other hand, it is slower when it is below the inversion point (oil continuous) as shown in in Figure 3.11. The smaller size of water droplets and high oil viscosity in W/O emulsions make the separation much slower than that in O/W emulsions.

CHAPTER 4

EMULSION RHEOLOGY AND ESP PERFORMANCE MODELING

This chapter presents an analytical study of emulsion rheology and the corresponding effect on ESP performance. The model was initially developed by Tulsa University Artificial Lift Projects (TUALP) and is improved in this section. The model is validated with the oil-water emulsion pump test results in Section 3.

4.1 Emulsion Rheology Model

Empirical correlations to predict emulsion rheology are available in the literature. Nevertheless, the accuracy of those models is only valid for pipe flow without considering the high shear flow environment. In ESP operation, the impeller rotation generates high shear inside the pump. Emulsion rheology depends on multiple factors, including fluid properties, the volumetric fraction of each phase, the droplet size distribution, operational temperature, shear rate, and the solids presented. The dimensionless analysis in Appendix B was performed based on the Buckingham Pi Theorem (1914) to investigate factors that influence the emulsion rheology.

The first attempt in emulsion rheology modeling is to define the inversion point, which corresponds the highest emulsion viscosity. In this study, emulsion correlations in Section 1 were compared. The Brinkman model was selected to unify the predictions of the effective viscosity and the inversion point with modified exponent (*E*):

$$\mu_E = \frac{\mu_C}{(1-\phi_D)^E}, \tag{4.1}$$

where μ_C is the continuous phase viscosity, ϕ_D is the volume fraction of the dispersed phase, and

E is determined by experiments. The effective viscosity μ_E at the inversion point can be expressed by continuous phase viscosity as:

$$\mu_E = \frac{\mu_o}{(1-\phi_w)^E} \quad , \tag{4.2}$$

$$\mu_E = \frac{\mu_w}{(1-\phi_o)^E} = \frac{\mu_w}{(\phi_w)^E} \quad . \tag{4.3}$$

Then,

$$\frac{\mu_o}{(1-\phi_w)^E} = \frac{\mu_w}{(\phi_w)^E}, \tag{4.4}$$

$$\frac{\mu_o}{\mu_w} = \frac{(1-\phi_w)^E}{(\phi_w)^E}, \tag{4.5}$$

The water fraction corresponding to the inversion point ϕ_{wI} can be obtained:

$$\phi_{wI} = \frac{1}{1+\tilde{\mu}^{1/E}}, \tag{4.6}$$

where $\tilde{\mu}$ is the viscosity ratio of oil and water.

The exponent (E) can be calculated from Equation (4.6) and experimentally measured inversion point. Thereafter, Equations (4.1) and (4.2) are used to compute the effective viscosity for the oil continuous region and water continuous region, respectively.

The dimensionless analysis prevails that three significant parameters need to be considered in the emulsion rheology model for an ESP, i.e., Weber number, Reynold number, and Strouhal number. The Weber number is introduced to reflect the droplet diameter effect on the emulsion rheology as:

$$We = \frac{\rho_A v^2 l}{\sigma} \cong \frac{\rho_A Q^2}{\sigma V}, \tag{4.7}$$

where ρ_A is the average density, Q is the flow rate, V is the pump channel volume of one stage, and σ is the interfacial tension between oil and water.

The droplet size and emulsion viscosity are affected by the level of turbulence. Therefore, Reynold number is used to consider the effect of turbulent mixing:

$$Re = \frac{\rho_A \, v \, l}{\mu_A} \cong \frac{\rho_A \, Q}{\mu_A \, d} \, , \tag{4.8}$$

where μ_A is the modeled emulsion viscosity and d is the representative pump diameter. The Reynold number can be calculated iteratively considering the change of modeled viscosity. The continuous phase viscosity μ_C can be used as a initial guess.

The change of pump rotational speed generates different shearing effects. Theoretically, the increase of rotational speed increases the shear rate and decreases the effective viscosity of the emulsion. Nevertheless, others may argue that the increase of the rotational speed creates smaller dispersed droplets at the blade tips and eventually increasing the effective viscosity of the emulsion. The phenomena will be investigated in the future with more tests on different pump rotational speeds. In this study, the dimensionless Strouhal number is proposed to reflect the rotational speed effect as:

$$St = \frac{f \, l}{v} \cong \frac{f \, V}{Q} \, , \tag{4.9}$$

where f is the ESP rotational speed. The final emulsion viscosity in the pump stage is calculated by Equation (4.10):

$$\mu_A = C \, (\, \mu_E \, - \, \mu_M \,) \, \mu_M \tag{4.10}$$

where μ_E is the effective viscosity obtained from Equations (4.2) and (4.3), μ_M is the mixture base viscosity which is defined as follow:

$$\mu_M = \frac{\mu_w}{(\, 1 - \phi_o \phi_{oE} \,)^E}, \tag{4.11}$$

$$\phi_{OE} = 1 - (\frac{\mu_w}{\mu_o})^{1/E}. \tag{4.12}$$

The correction factor C in Equation (4.10) is introduced to correlate dimensionless numbers

We, *Re*, and *St*:

$$C = \frac{(N\,We\,Re)^n}{b\,St^m}. \tag{4.13}$$

N represents the number of pump stages, *b*, *n*, and *m* are the coefficients obtained from the experiments data. In this study, Equation (4.13) can be expressed as:

$$C = \frac{(14\,We\,Re)^{0.1}}{10\,St^{0.2}}. \tag{4.14}$$

Finally, the emulsion viscosity in this study is calculated by:

$$\mu_A = \frac{(14\,We\,Re)^{0.1}}{10\,St^{0.2}}\,(\,\mu_E\,-\,\mu_M\,)\,\mu_M. \tag{4.15}$$

4.1.1 Model Comparison with Experiment Data

Figure 4.1 shows the proposed model prediction against the experiment results under different oil viscosities. The emulsion viscosity is higher with higher oil viscosity. In general, the model predictions of emulsion viscosity are mostly within ±10% discrepancy compared with the experiment data as shown in Figure 4.2.

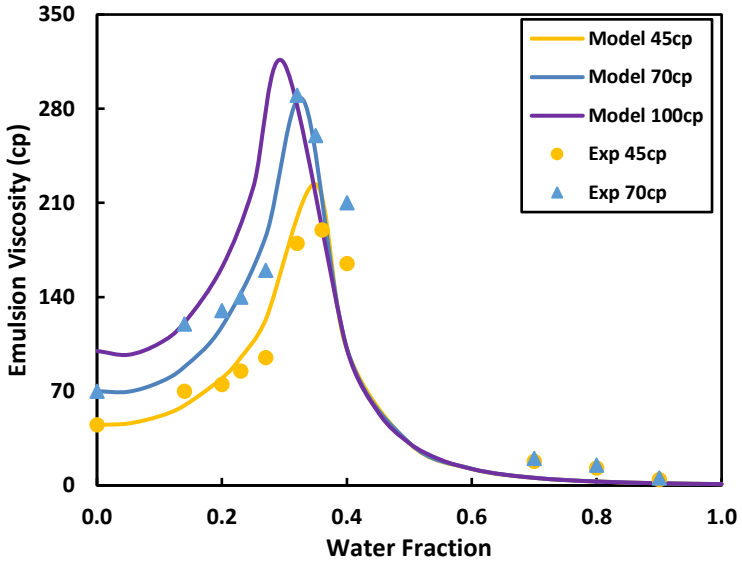

Figure 4.1: Emulsion Rheology Model Compared with Experiment Data

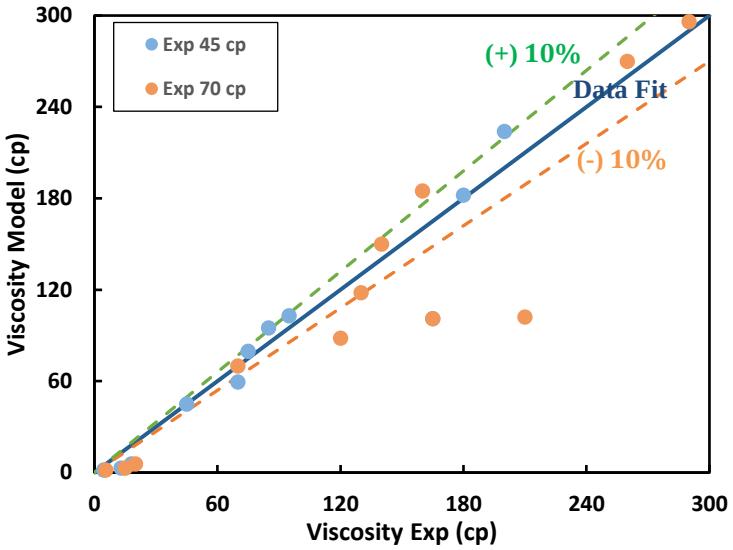

Figure 4.2: Error Analysis of Emulsion Rheology Model

The proposed model gives reasonable predictions, especially in the oil continuous region. However, it over-predicts the emulsion viscosity in the water continuous region. It may be due to the loss of emulsion stability in the water continuous region, especially at low flow rates.

4.2 ESP Performance Model

This section presents the mechanistic ESP performance model developed at Tulsa University Artificial Lift Projects (TUALP). The proposed emulsion rheology model is incorporated into the ESP model to establish the two-phase oil/water emulsion ESP model, which has been compared with the experimental data presented in Section 3.

The mechanistic model was initially developed based on the Euler Equation for the centrifugal pump, and the potential energy losses in the pump are modeled analytically. The modeling approach starts with a best match flow rate (Q_{BM}) concept. At Q_{BM} the flow direction at the impeller outlet matches the designed flow direction of the pump diffuser. The mismatch of flow directions generates recirculation loss in the impeller. The actual pump boosting pressure is

the diminished ideal pump boosting pressure due to losses including friction loss, recirculation loss, turn loss, and leakage loss. Figure 4.3 shows the theoretical pump performance and losses that are incorporated in this study.

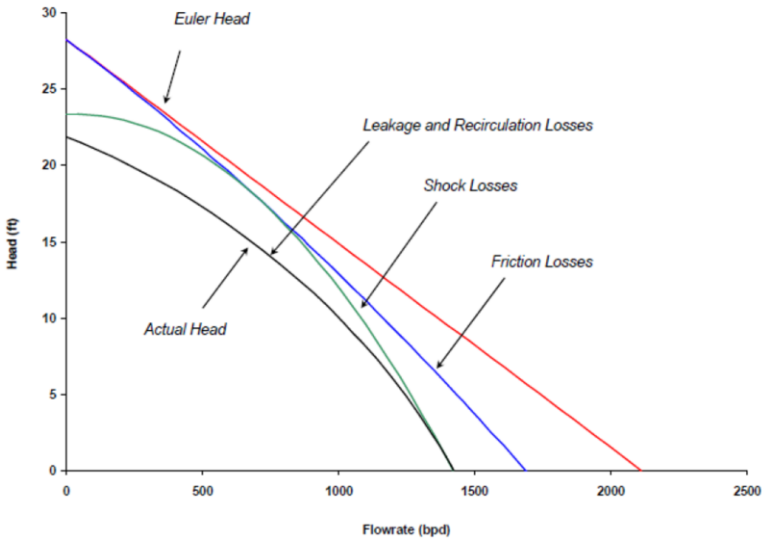

Figure 4.3: Theoretical ESP Pump Performance and Losses

4.2.1 EulerEquation for ESP Impeller

Euler's theory is based upon the conservation law of angular momentum under the ideal assumption in a rotating flow field, i.e., incompressible fluid, frictionless flow, infinite number of blades, and static flow field. Figure 4.4 displays the velocity components at the impeller inlet and outlet.

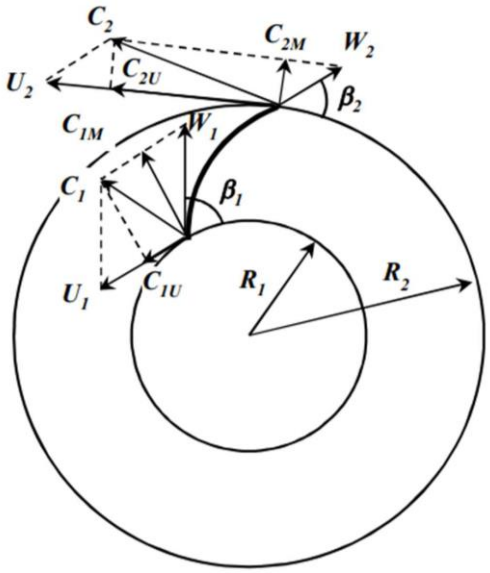

Figure 4.4: Velocity Triangles at Impeller Inlet and Outlet

R_1 is the radius of the impeller inlet. R_2 is the radius of the impeller outlet. β_1 is the blade angle from tangential at the impeller inlet. β_2 is the blade angle from tangential at the impeller outlet. U_1 is the impeller tangential velocity at the inlet. U_2 is the impeller tangential velocity at the outlet. W_1 is the fluid relative inlet velocity along the impeller surface. W_2 is the fluid relative outlet velocity along the impeller surface. C_1 is the absolute fluid velocity at the impeller inlet. C_2 is the absolute fluid velocity at the impeller outlet. C_{1M} is the meridional velocity at the impeller inlet. C_{2M} is the meridional velocity at the impeller outlet. C_{1U} is the fluid tangential velocity at the impeller inlet. and C_{2U} is the fluid tangential velocity at the impeller outlet.

The fluid flow in an ESP stage is the product of the external torque acting on the impeller. The external torque can be derived from Newton's second law of motion in Equation (4.16):

$$\tau = \dot{m}\,(R_2 C_{2u} - R_1 C_{1u}). \tag{4.16}$$

The impeller tangential velocity at the inlet and the outlet can be expressed as:

$$U_1 = R_1\,\Omega, \tag{4.17}$$

$$U_2 = R_2\,\Omega, \tag{4.18}$$

where Ω is the angular velocity of the impeller, which is calculated with the pump rotational speed (*N*) and can be expressed as:

$$\Omega = \frac{2\,\pi\,N}{60}. \tag{4.19}$$

Then, the shaft power can be calculated by adopting the equations above as:

$$P_2 = \rho\,Q\,(U_2C_{2u} - U_1C_{1u}). \tag{4.20}$$

The hydraulic power can be written as:

$$P_{hyd} = H_E\,\rho\,g\,Q. \tag{4.21}$$

Under the assumption of no losses during the fluid flow, Equation (4.20) equals Equation (4.21). Then, the Euler's Head can be expressed as follow:

$$H_E = \frac{(U_2C_{2u} - U_1C_{1u})}{g}. \tag{4.22}$$

According to the velocity trigonometry, the Euler's Head can be rewritten as follow:

$$H_E = \frac{{U_2}^2 - {U_1}^2}{2g} + \frac{{W_2}^2 - {W_1}^2}{2g} + \frac{{C_2}^2 - {C_1}^2}{2g}. \tag{4.23}$$

The first term reflects the static head due to the centrifugal forces, the second term reflects the static head due to the velocity change, and the third term is the dynamic head.

The fluid absolute velocity is defined as meridional velocity, which can be expressed as:

$$C_{1M} = \frac{Q + Q_{LK}}{(2\pi R_1 - Z_I\,T_B)y_{I1}}, \tag{4.24}$$

$$C_{2M} = \frac{Q + Q_{LK}}{(2\pi R_2 - Z_I\,T_B)y_{I2}}. \tag{4.25}$$

where Q is the flow rate, Q_{LK} is the leakage flow rate, Z_I is the impeller blade number, T_B is the blade thickness projected to the radial direction, y_{I1} is the impeller inlet height and y_{I2} is the impeller outlet height.

The relative velocity at the impeller inlet and the impeller outlet can be expressed as:

$$W_1 = \frac{C_{1M}}{Sin\ \beta_1}, \tag{4.26}$$

$$W_2 = \frac{C_{2M}}{Sin\ \beta_2}, \tag{4.27}$$

The fluid absolute velocities at the impeller inlet and outlet can be expressed as:

$$C_1 = \sqrt{C_{1M}^2 + (U_1 - \frac{C_{1M}}{tan\ \beta_1})^2}\ , \tag{4.28}$$

$$C_2 = \sqrt{C_{2M}^2 + (U_2 - \frac{C_{2M}}{tan\ \beta_2})^2}\ . \tag{4.29}$$

The fluid tangential velocities at the impeller inlet and outlet can be expressed as:

$$C_{1U} = U_1 - W_1 \cos\beta_1, \tag{4.30}$$

$$C_{2U} = U_2 - W_2 \cos\beta_2. \tag{4.31}$$

Then, Equation (4.22) can be expanded as:

$$H_E = \frac{U_2(U_2 - W_2 \cos\beta_2 - U_1(U_1 - W_1 \cos\beta_1}{g}, \tag{4.32}$$

Under the assumption of no tangential fluid velocity at the impeller inlet as shown in Figure 4.5, C_{1U} = 0, C_1= C_{1M}, and the Euler Equation under this assumption can be expressed as:

$$H_E = \frac{U_2^2}{g} + \frac{U_2\, C_{2M}}{\mathrm{g}\tan\beta_2}. \tag{4.33}$$

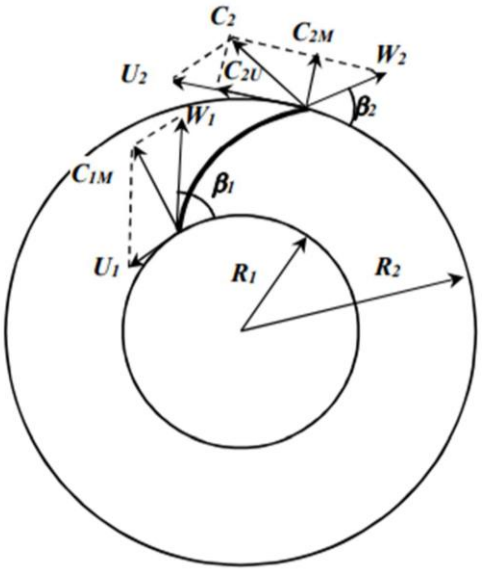

Figure 4.5: Velocity Triangles at Impeller Inlet and Outlet without Inlet Rotation

4.2.2 Correction Factor for Theoretical Head

Wiesner (1967) proposed an empirical correlation for slip factor (δ_s) as a correction factor for Euler's Head to adjust the mismatch of real outlet velocity with the designed outlet velocity. The slip factor was introduced into the Euler's Equation, and the theoretical head can be expressed as:

$$H_{th} = \delta_s \frac{U_2^2}{g} + \frac{U_2\, C_{2M}}{\mathrm{g}\tan\beta_2}, \tag{4.34}$$

where δ_s can be expressed as an empirical correlation:

$$\delta_s = 1 - \frac{\sqrt{\sin\beta_2}}{{Z_I}^{0.7}}, \tag{4.35}$$

Zhang (2017) modified the slip correction factor to better match the experiment data as:

$$\delta_s = 1 - \frac{\sqrt{\sin \beta_2}}{Z_I^{1.5} \left(\frac{N_{S,ref}}{N_S}\right)^{0.4}}, \tag{4.36}$$

where the $N_{S,ref}$ is the reference specific speed, and in the proposed model $N_{S,ref}$ is equal to 3448. Then, Equation (4.34) can be expanded to express the theoretical head versus angular velocity as:

$$H_{th} = \delta_s \frac{\Omega^2 r_2^2}{g} + \frac{Q\,\Omega}{2\,\pi\,g\,h\,\tan\beta_2}. \tag{4.37}$$

4.2.3 Effective Velocity at Impeller Outlet

The best match flow rate (Q_{BM}) is assumed to have the same fluid absolute velocity direction at the impeller outlet with the direction of the designed flow from the impeller to the diffuser. When ESP is operated at other flow rates, an effective velocity is introduced to illustrate the flow rate alteration. Figure 4.6 shows the velocity profile at the impeller outlet when the operating flow rate is lower than Q_{BM}.

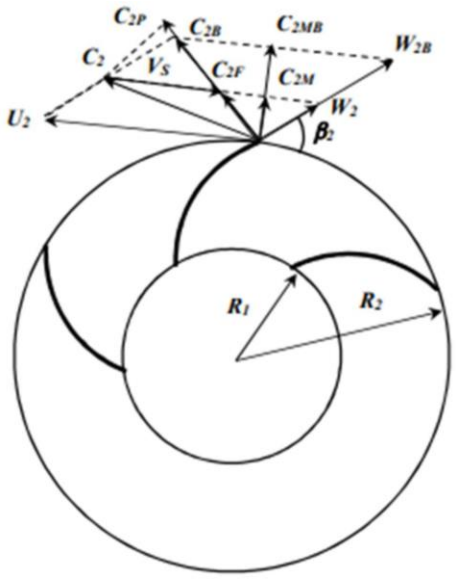

Figure 4.6: Velocity Triangles at Impeller Outlet when $Q + Q_{LK} < Q_{BM}$

If the operating flow rate is lower than Q_{BM}, the fluid flow velocity outside the impeller can be expressed as:

$$C_{2F} = C_{2B} \frac{Q}{Q_{BM}}, \tag{4.38}$$

where C_{2B} is the absolute fluid velocity at the impeller outlet corresponding to Q_{BM}.

When C_{2F} is higher than C_2, the shear velocity V_S is defined as:

$$V_S = U_2 \frac{Q_{BM} - (Q + Q_{LK})}{Q_{BM}}. \tag{4.39}$$

The projections of C_2 and V_S on the perpendicular direction of C_{2B} are the same, which can be written:

$$C_2^2 - C_{2P}^2 = V_S^2 - (C_{2P} - C_{2F})^2. \tag{4.40}$$

From Equation (3.40), C_{2P} can be solved as:

$$C_{2P} = \frac{C_2^2 + C_{2F}^2 - V_S^2}{2\, C_{2F}}. \tag{4.41}$$

Figure 4.7 illustrates the recirculation flow in the impeller due to the high shear effect. In addition, the theoretical kinetic energy is not fully transformed into static pressure. Recirculation flow is affected by many factors, including shear velocity, impeller channel size, and fluid viscosity. In this study, the Reynolds number is introduced to estimate the recirculation effect:

$$Re_c = \frac{\rho\, V_S\, D_C}{\mu}, \tag{4.42}$$

where D_C is the representative impeller channel width at the outlet, which can be computed by:

$$D_c = \frac{2\,\pi\,R_2}{Z_I}\sin\beta_2 - T_B. \tag{4.43}$$

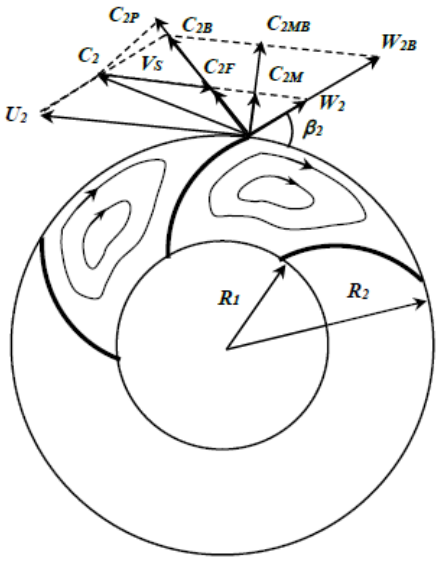

Figure 4.7: Recirculation Flow in Impeller

The effective velocity alteration due to the recirculation effect is taken into account in the mechanistic model by introducing the velocity reduction factor as:

$$\sigma = \frac{(\frac{\mu_w}{\mu_o})^{0.1}}{1+0.02Re_c^{0.2}}\,. \tag{4.44}$$

Empirical correlation of effective velocity is developed based on experiments as:

$$C_{2E} = C_{2F} + \sigma\,(C_{2P} - C_{2F})\,. \tag{4.45}$$

ESP can be operated at a flow rate that is higher than Q_{BM}. The velocity components at the pump impeller outlet are then displayed in Figure 4.8. In this scenario, the shear velocity is calculated as:

$$V_S = U_2\,\frac{(Q+Q_{LK}) - Q_{BM}}{Q_{BM}}. \tag{4.46}$$

The calculation steps and equations are the same as the scenario when the operating flow rate is lower than Q_{BM}. Eventually, the effective Euler's Head can be defined by considering the recirculation effect in the impeller as:

$$H_{EE} = H_E + \frac{C_{2E}^2 - C_2^2}{2g}. \tag{4.47}$$

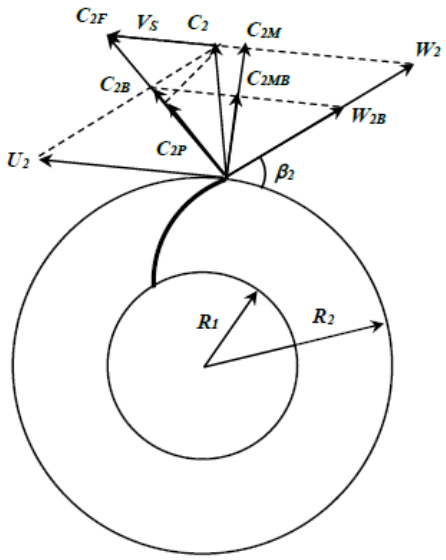

Figure 4.8: Velocity Triangles at Impeller Outlet when $Q + Q_{LK} > Q_{BM}$

4.2.4 Pressure Losses

4.2.4.1 Recirculation Loss

The recirculation loss is derived from the mismatch of velocity triangles when the pump flow rate derivates from Q_{BM}. Q_{BM} is tuned by matching the predicted water curve to the manufacturer catalog.

The derivation of recirculation loss is provided in the previous sub-section, and can be expressed as:

$$H_{recirculation} = \frac{C_2^2 - C_{2E}^2}{2g}. \quad (4.48)$$

4.2.4.2 Friction Loss

The friction factor in an ESP is calculated by Sun and Prado (2006) correlation in Equation (4.49). The equation is based on Churchill (1977) friction factor correlation in Equation (4.50) and accounts for the channel shape effect, F_γ, blade curvature effect, F_β, and pump rotational speed effect, F_ω.

$$f_{\gamma\beta\omega} = f\ F_\gamma\ F_\beta\ F_\omega, \quad (4.49)$$

where f Churchill's (1977) friction factor correlation is defined as

$$f = 2\ [(\frac{8}{Re})^{12} + \frac{1}{(A+B)^{1.5}}]^{1/12}, \quad (4.50)$$

$$A = [\ 2.457\ln\{\frac{1}{(\frac{7}{Re})^{0.9} + 0.27(\frac{\varepsilon}{D})}\}]^{16}\ , \quad (4.51)$$

and

$$B = (\frac{37530}{Re})^{16}. \quad (4.52)$$

The Reynolds number is

$$Re = \frac{d_H Q_L \rho_L}{2\pi r \mu_L \sin\beta}. \quad (4.53)$$

Sun and Prado (2006) proposed channel shape effect (F_γ) as:

$$F_\gamma = \left[\frac{2}{3} + \frac{11}{24} l_L (2 - l_L)\right]^{-1} \quad Re \leq 2300 \quad (4.54)$$

and

$$F_\gamma = \left[\frac{2}{3} + \frac{11}{24} l_L (2 - l_L)\right]^{-0.25} \quad Re \leq 2300 \ , \tag{4.55}$$

where the aspect ratio of the rectangular cross-section is defined as

$$l_L = \frac{min(a_L, b_L)}{max(a_L, b_L)}, \tag{4.56}$$

where a_L is the channel width, and b_L is the channel height for the impeller or diffuser.

The pipe curvature effect F_β is based on the critical Reynolds number to consider the laminar and turbulent effects. The proposed Reynolds numbers are defined as:

$$N_{Re} = 2 \times 10^4 \times \left(\frac{R_c}{r_H}\right)^{-0.32} \quad \frac{R_c}{r_H} < 860 \ , \tag{4.57}$$

$$N_{Re} = 2300 \quad \frac{R_c}{r_H} < 860 \ , \tag{4.58}$$

where R_c is the radius of curvature along the flow channel, and r_H is the hydraulic radius based on the hydraulic diameter that is defined as:

$$R_c = \frac{1}{\sin\beta} \frac{1}{-\frac{d\beta(r)}{dr} + \frac{1}{r \tan\beta}}, \tag{4.59}$$

$$r_H = \frac{d_H}{2} . \tag{4.60}$$

The pipe curvature effect F_β in laminar region when $Re < N_{Re}$ can be expressed as:

$$F_\beta = 0.266\, Re^{0.389} \left(\frac{R_c}{r_H}\right)^{-0.1945} . \tag{4.61}$$

In turbulent region when $Re > N_{Re}$, F_β can be expressed as:

$$F_\beta = \begin{cases} \left(Re\left(\frac{R_c}{r_H}\right)^{-2}\right)^{0.05} & Re\left(\frac{R_c}{r_H}\right)^{-2} \geq 300 \\ 0.092\left(Re\left(\frac{R_c}{r_H}\right)^{-2}\right)^{0.25} + 0.962 & 300 \geq Re\left(\frac{R_c}{r_H}\right)^{-2} > 0.034 \\ 1 & Re\left(\frac{R_c}{r_H}\right)^{-2} \leq 0.034 \end{cases}. \quad (4.62)$$

In addition, the critical Reynolds number is re-defined when considering the rotational speed effect F_ω. The proposed Reynolds numbers for the rotational speed effect are:

$$N_{Re} = 1070(Re_\omega)^{0.23} \qquad Re_\omega \geq 28, \quad (4.63)$$

$$N_{Re} = 2300 \qquad Re_\omega < 28, \quad (4.64)$$

where Reynolds number Re_ω is given by:

$$Re_\omega = \frac{\omega d_H^2 \rho_l}{\mu_l}. \quad (4.65)$$

The rotational speed effect F_ω for laminar flow when $Re < N_{Re}$ can be expressed as:

$$F_\omega = \begin{cases} 1 & Re\,Re_\omega \leq 220 \; and \; \frac{Re_\omega}{Re} < 0.5 \\ 0.0883\,Re\,Re_\omega^{0.25}\left(1 + 11.2\left(Re\,Re_\omega^{-0.325}\right)\right) & 220 < Re\,Re_\omega < 10^7 \; and \; \frac{Re_\omega}{Re} < 0.5 \\ \frac{0.0672 Re_\omega^{0.5}}{1 - 2.11 Re_\omega^{-0.5}} & \frac{Re_\omega}{Re} \geq 0.5 \end{cases} \quad (4.66)$$

The rotational speed effect F_ω for turbulent flow when $Re > N_{Re}$ can be expressed as:

$$F_\omega = \begin{cases} 1 & \frac{Re_\omega^2}{Re} < 1 \\ 0.942 + 0.058\left(\frac{Re_\omega^2}{Re}\right)^{0.282} & 1 < \frac{Re_\omega^2}{Re} < 15 \\ 0.942\left(\frac{Re_\omega^2}{Re}\right)^{0.05} & \frac{Re_\omega^2}{Re} > 15 \end{cases}. \quad (4.67)$$

Based on the friction factor correlation in Equation (4.49), the friction loss can be expressed as:

$$H_{friction} = \frac{f_{\gamma\beta\omega} Q^2}{8 g D_H \pi^2 b_m^2 \sin^3\beta_m} \frac{r_2 - r_1}{r_1 r_2}. \quad (4.68)$$

4.2.4.3 Turn Loss

The turn loss is affected by the alteration of flow directions from the impeller outlet to the diffuser inlet and from the diffuser outlet to the impeller inlet of the next stage:

$$H_{TI} = f_{TI}\frac{V_I^2}{2g}, \tag{4.69}$$

$$H_{TD} = f_{TD}\frac{V_D^2}{2g}, \tag{4.70}$$

where f_{TI} and f_{TD} are the local drag coefficients, which are determined based on the experimental data. Then, the total turn loss is

$$H_{turn} = f_{TI}\frac{V_I^2}{2g} + f_{TD}\frac{V_D^2}{2g}. \tag{4.71}$$

4.2.4.4 Leakage Loss

The leakage loss is caused by a liquid back flow through the clearance between impeller and diffuser. Tuzson (2000) analyzed the leakage loss in a rotating centrifugal pump by outlining the flow path as shown in Figure 4.9. In an ESP, the reverse flow is most likely to flow through the secondary leakage flow channel, including the balance holes and the clearance between the impeller and the diffuser.

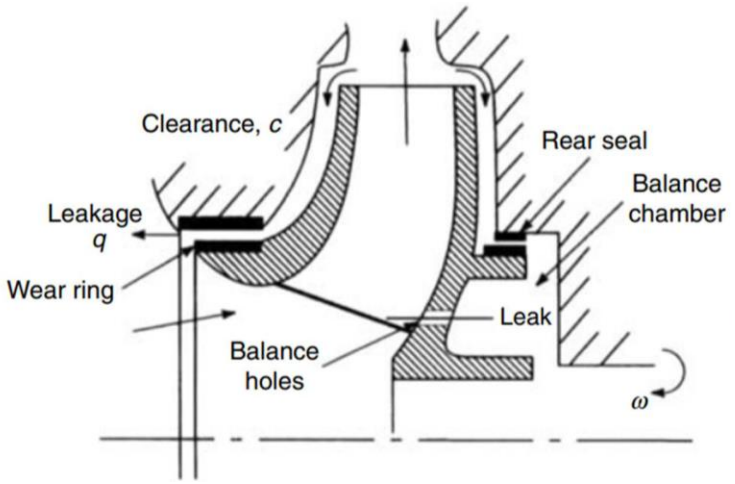

Figure 4.9: ESP Leakages through Balance Holes and Clearance (Tuzson 2000)

The head loss due to leakage flow can be estimated by considering the contraction and expansion of the flow through the clearance passage:

$$H_{leakage} = f_c \frac{V_L^2}{2g} + f_E \frac{V_L^2}{2g} + f_{LK} \frac{V_L^2 L_G}{2g\, S_L}, \tag{4.72}$$

where V_L is the fluid velocity when passing through the clearance, f_c, f_E, f_{LK}, are the friction factors coefficient due to contraction, expansion, and friction. L_G is the leakage channel length, S_L is the leakage width. Figure 4.10 describes the leakage geometries in an ESP Stage.

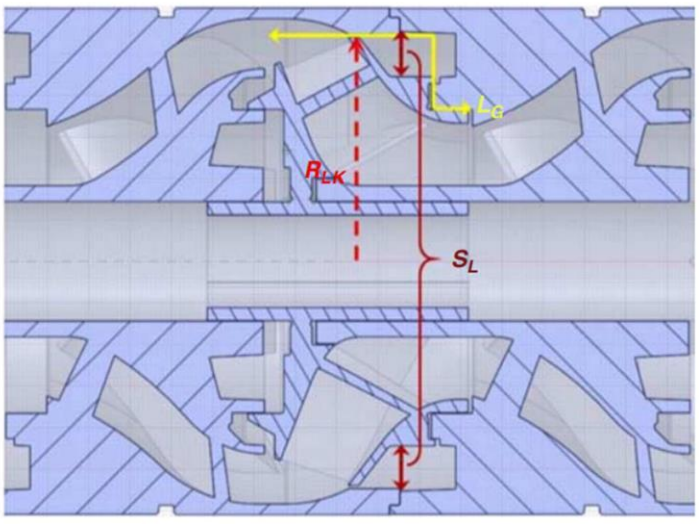

Figure 4.10: Leakage Geometries in an ESP Stage

The fluid velocity can be calculated by Equation (4.73) as:

$$V_L = \sqrt{\frac{2gH_{leakage}}{f_{LK}\frac{L_G}{S_L} + f_c + f_E}}. \tag{4.73}$$

Then, the leakage flow rate can be calculated as:

$$Q_{LK} = 2\pi R_{LK} S_L V_L, \tag{4.74}$$

where R_{LK} is the radius of leakage clearance. The leakage flow rate Q_{LK} must be accounted into the total liquid flow rate in a rotating ESP. For iteration purpose, a simple formula is proposed in this study to estimate head loss due to leakage as:

$$H_{leakage} = H_{EE} - H_{recirculation} - H_{friction} - H_{turn} - \frac{U_2^2 - U_{LK}^2}{8g}, \tag{4.75}$$

where U_{LK} is tangential velocity due to the impeller rotation at the leakage passage, which can be expressed as:

$$U_{LK} = R_{LK}\Omega. \tag{4.76}$$

Assuming the actual ESP head and the leakage flow rate, the leakage loss is computed by an iterative process based on Equations (4.72) and (4.75). The relative errors are used to check if the calculation is converged or not by comparing it with the convergence criterion.

4.3 Mechanistic Model Setup

The mechanistic model comprises of emulsion rheology model and the ESP boosting pressure prediction model. The emulsion rheology model is incorporated into the pump boosting pressure prediction model. The result of the new mechanistic model is compared with the experimental data under different operation conditions. Figure 4.11 shows the flow chart of the mechanistic model.

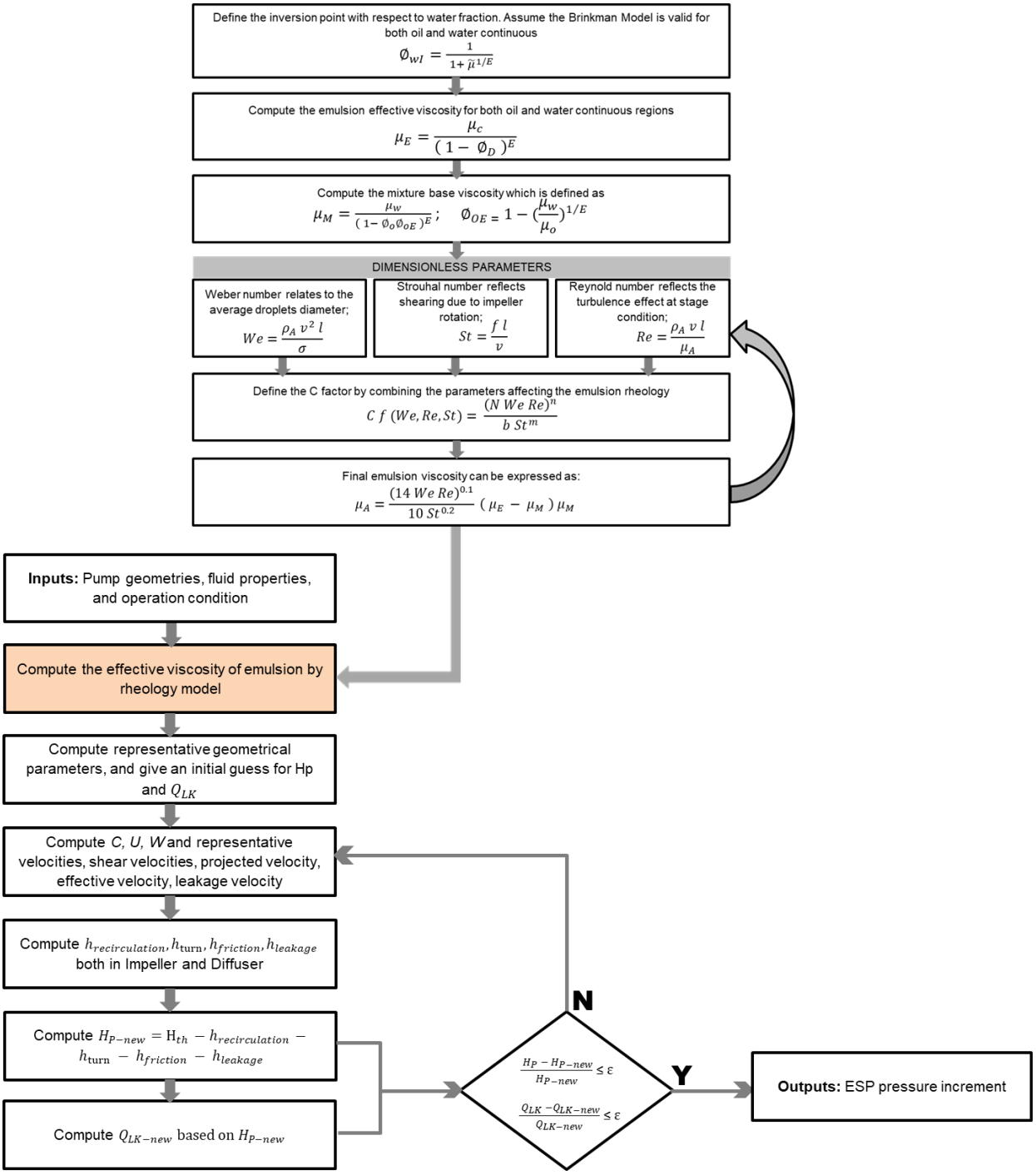

Figure 4.11: Mechanistic Model Flow Chart

The model is written in the computer language program Python. Fluid properties, pump geometries, and operating conditions are inputs.

In this study, the best match flow rate (Q_{BM}) must be determined at the beginning. It is performed by a tuning process in which the model predicted water curve matches well with that provided by the manufacturer. An arbitrary value of the best match flow rate (Q_{BM}) is given as an initial guess. By adjusting the value of the best match flow rate (Q_{BM}), different comparisons can be made as shown in Figure 4.12. Q_{BM} of 5000 bpd agrees best with the catalog. Q_{BM} should be corrected when applying to the high viscosity fluid flow or oil/water emulsion flow conditions. An empirical correlation is introduced based on the experimental data.

$$\frac{Q_{BM}}{(Q_{BM})_{water,BEP}} = \frac{N}{N_{BEP}} \left(\frac{\mu_l}{\mu_w}\right)^n \tag{4.77}$$

where n = 0.01 – 0.16, depending on the specific speed of an ESP.

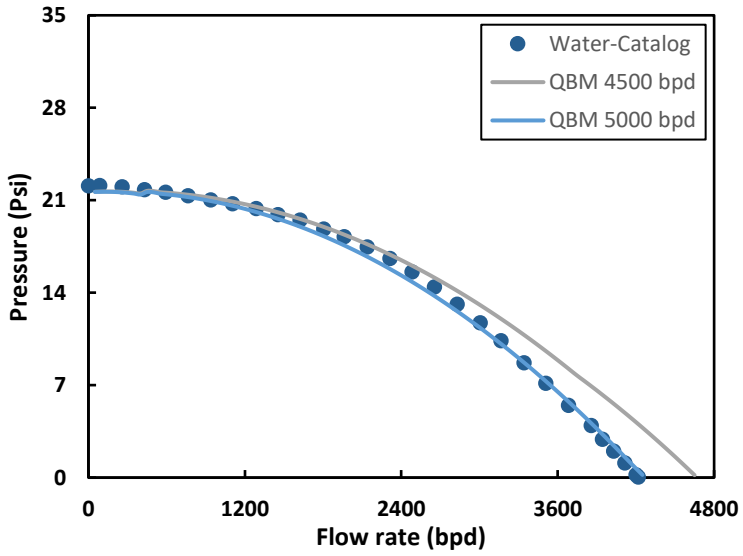

Figure 4.12: Tuning Mechanistic Model to Catalog Water Curve at 3000 RPM

4.4 Mechanistic Model Validation

The experimental data are compared with the predicted results to validate the proposed mechanistic model in this study. Statistical definitions of errors are used to demonstrate the performance of the mechanistic model by comparing the model predicted ESP boosting pressure

against the corresponding experimental data (Wang et al. 2014). The statistical definitions of errors are explained in Appendix C.

4.4.1 Single Phase VG-320 Oil

The mechanistic model is validated by experimental data of TE-2700 for different oil viscosities ranging from 45 cp to 105 cp at the pump rotational speed of 3,000 RPM, and 3,500 RPM. The mechanistic model results agree well with the experiment data as shown in Figures 4.13 - 4.15 with ±15% data discrepancy, which proves the accuracy of the mechanistic model.

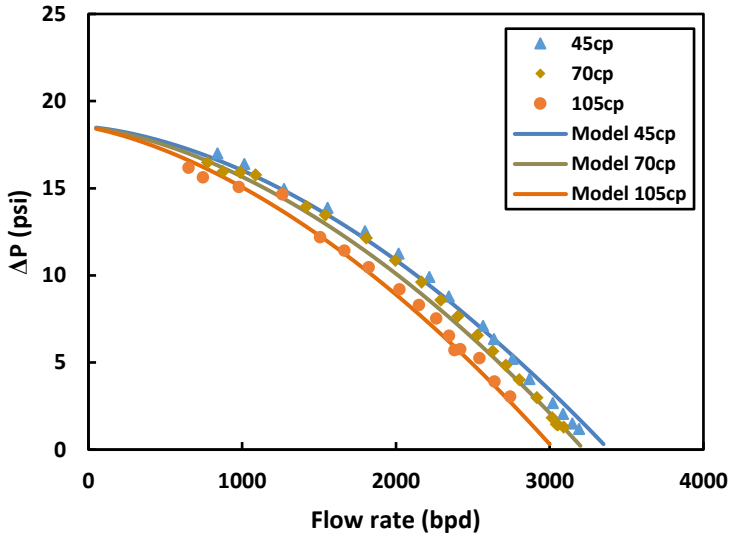

Figure 4.13: Comparison of Mechanistic Model and Experimental Data at 3000 RPM

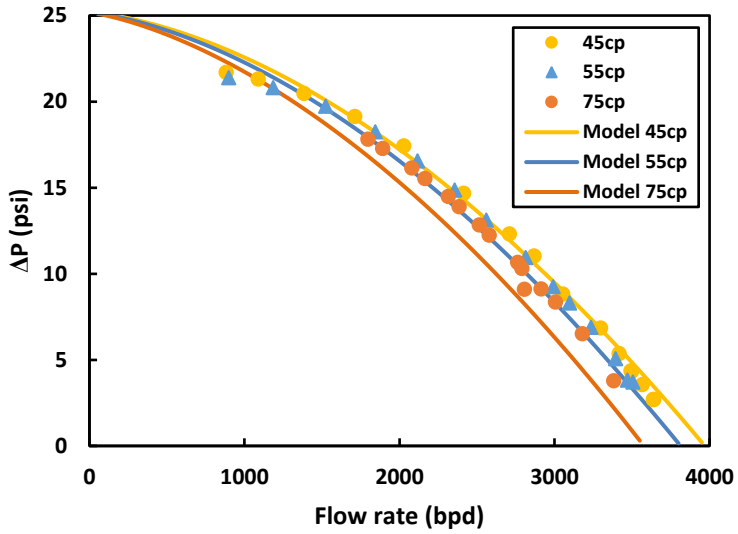

Figure 4.14: Comparison of Mechanistic Model and Experimental Data at 3500 RPM

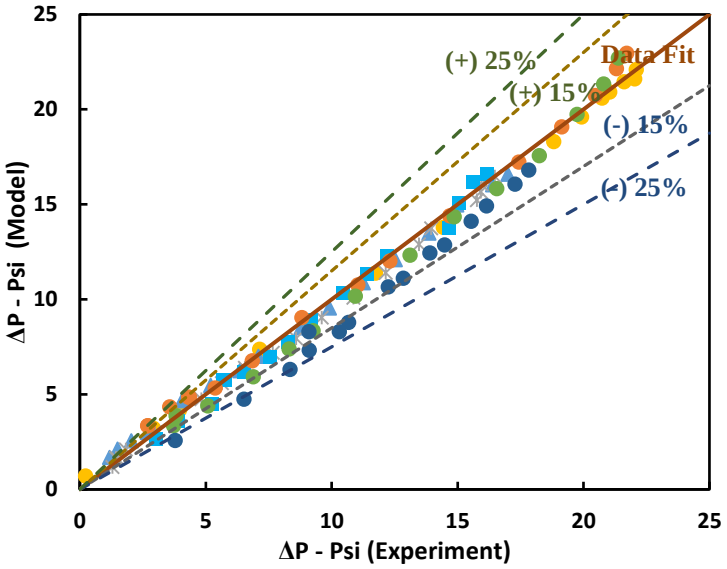

Figure 4.15: Error Analysis of Mechanistic Model for Single Phase Oil

4.4.2 Oil/Water Emulsion

The mechanistic model of oil/water emulsion is validated by experimental data of TE-2700 with two oil viscosities, i.e., 45 cp and 70 cp, at the pump rotational speed of 3,000 RPM. The mechanistic model results agree well with the experiment data in Figures 4.16 - 4.19, in which the

discrepancy is bounded within the ±15% error bars. Higher data discrepancy prevails when water fraction is close to the phase inversion point, which is presumably due to the unstable flow characteristics of oil-water emulsion around the inversion point.

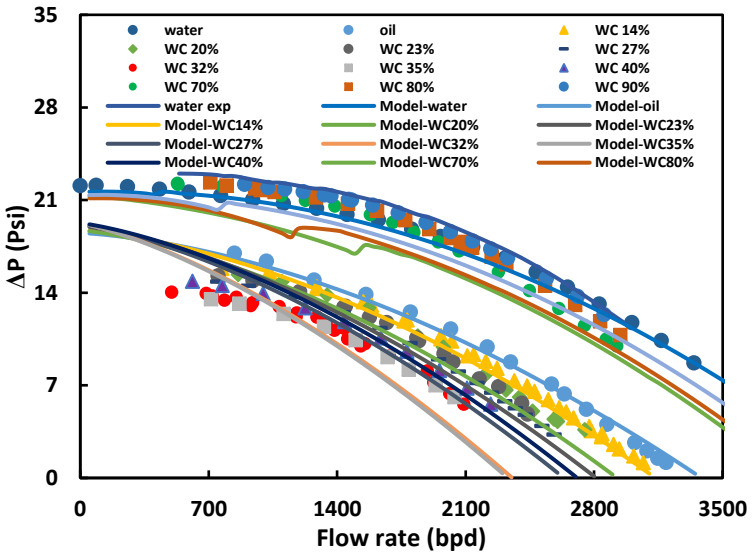

Figure 4.16: Comparison of Mechanistic Model and Experimental Data for Oil/Water Emulsion with 45 cp Oil Viscosity at 3000 RPM

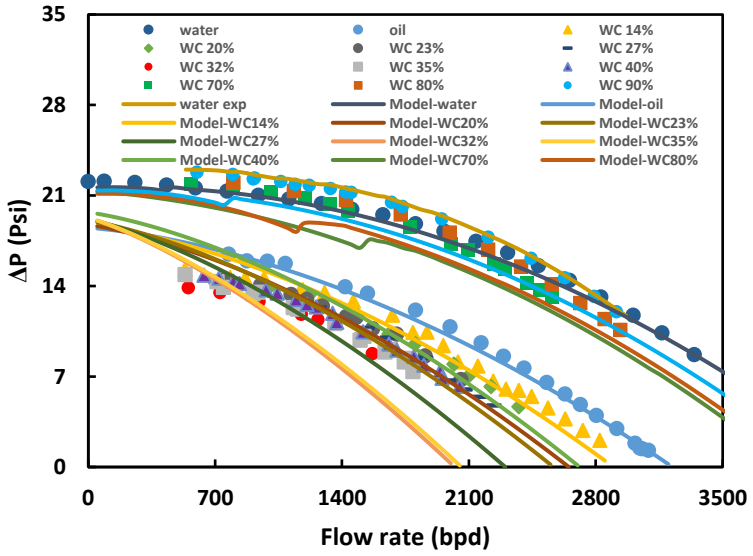

Figure 4.17: Comparison of Mechanistic Model and Experimental Data for Oil/Water Emulsion with 70 cp Oil Viscosity at 3000 RPM

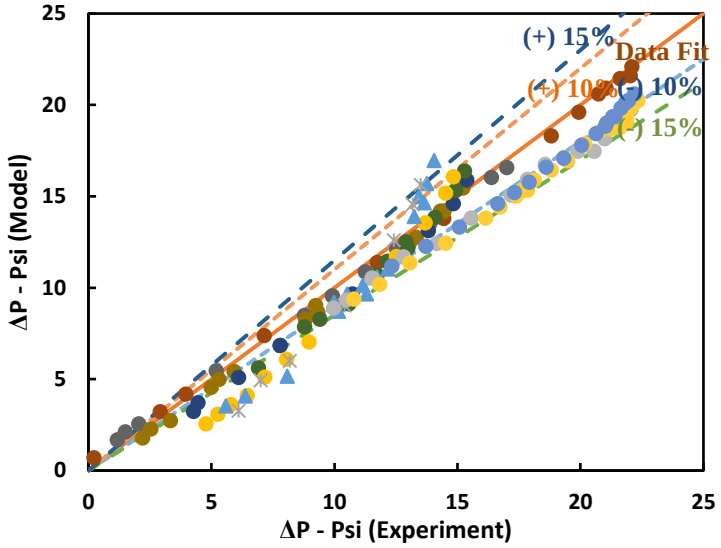

Figure 4.18: Error Analysis of Mechanistic Model for Oil/Water Emulsion with 45 cp Single Phase Oil Viscosity

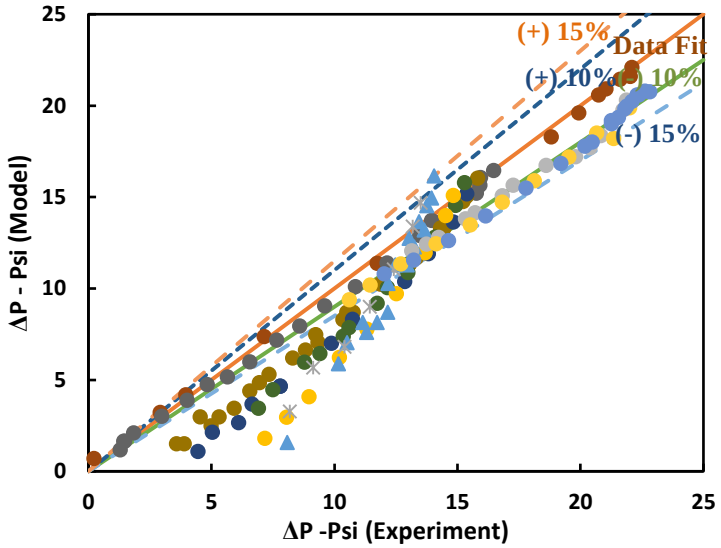

Figure 4.19: Error Analysis of Mechanistic Model for Oil/Water Emulsion with 70 cp Single Phase Oil Viscosity

4.4.3 Statistical Errors

In this chapter, two categories of errors, namely the relative error and the actual error, are defined as:

$$e_i = \frac{P_{model} - P_{exp}}{P_{exp}} 100\%, \tag{4.76}$$

and

$$e_j = P_{model} - P_{exp}. \tag{4.76}$$

Based on the relative error and actual error, six statistical parameters are defined, i.e., average relative error (ε_1), absolute average relative error (ε_2), standard deviation of relative error (ε_3), average actual error (ε_4), absolute average actual error (ε_5), and standard deviation of actual error (ε_6). Table 4.1 lists the statistical errors for both single-phase oil experiments and oil/water emulsion experiments. The average absolute relative error and standard deviation of mechanistic model predictions compared to the experimental data for both single-phase oil and oil/water emulsion are less than 20%, which indicates good agreement of the mechanistic model with experimental results. Unlike the empirical correlations that require experimental data points as the input (Ofuchi et al. 2017; Zhu et al. 2019a), the proposed mechanistic model only needs the water performance curves provided by the pump manufacturer catalog.

Table 4.1. Statistical Errors of Model and Data Comparisons

Error Analysis	ε_1 (%)	ε_2 (%)	ε_3 (%)	ε_4 (psi)	ε_5 (psi)	ε_6 (psi)
Single Phase Oil	-1.6	7.8	11.7	-0.32	0.58	0.70
Oil/water Emulsion	-12.6	15.3	16.4	-1.4	1.6	1.4

CHAPTER 5

CONCLUSIONS AND RECOMMENDATIONS

At present, emulsion rheology in the ESP is still not well understood. The industry relies on empirical correlations, which are only applicable for pipe flows without considering the shear effect. This study presents the experimental investigation of emulsion rheology and the model development for the emulsion rheology inside the ESP, as well as its effect on the pump performance. The conclusions and recommendations are summarized below.

5.1 Conclusions

The conclusions of this study are presented in two parts, the experimental study and the development of the mechanistic models.

5.1.1 Experimental Study

- The emulsion effective viscosity as a function of water fraction has been investigated considering the shear effect, droplet size, and turbulent mixing. Starting from single-phase oil, the emulsion effective viscosity increases with the increase of water fraction until the inversion point, after which the viscosity decreases. The ESP performance deteriorates with fluid viscosity increase.
- The increase of emulsion effective viscosity in the water-oil flow through an ESP induces higher pressure loss in the pump due to higher friction.

- Phase inversion is observed at 35% and 32% water fractions for oil viscosities 45 cp and 70 cp, respectively. The lower oil viscosity corresponds to a higher phase inversion water fraction. Therefore, it is essential to set the appropriate range of operational conditions away from the inversion point. A better understanding of the emulsion rheology can help provide an optimized ESP design for oil and water production.

5.1.2 Model Development

- Turbulence effect, droplet size effect, and shearing effect are the major parameters affecting emulsion rheology. The emulsion rheology model is compared with experiment results.
- The discrepancies for different oil viscosities are mostly within ±10%. The new model predictions are good especially in the oil continuous region. However, it over-predicts the emulsion viscosity in the water continuous region since the emulsion loses its stability, especially at low flow rates.
- The oil/water emulsion rheology model is incorporated in the ESP mechanistic model for boosting pressure prediction. The predicted boosting pressures agree well with the experiment data, bounded by ±15% error lines. The statistic relative error and standard deviation of the data are less than 20%, which validates the applicability and the accuracy of the proposed mechanistic model.
- The proposed mechanistic model is valuable to field applications, including optimizations of production system design and operation. Unlike previous empirical correlations, the mechanistic model can be used for different flow conditions as long as the pump geometry and water curve are available from the manufacturers.

5.2 Recommendations

The following are several recommendations for future studies:

- More experiment data may be acquired to valiate the models using new types of oil with wider viscosity range and different ESPs.
- The pipe-in-pipe heat exchanger needs to be improved to maintain the loop temperature more effectively.
- Either shorten the loop or add a boosting pump to handle the high-pressure loss in the experimental loop, especially for high viscosity tests.
- Additional experiments with different pump rotational speeds are recommended to investigate the pump rotational speed effect on emulsion viscosity.

NOMENCLATURE

BEP	best efficiency point
DAQ	data acquisition system
ESP	electric submersible pump
PV	pipe viscometer
VSD	variable speed drive
A_{SD}	diffuser channel total wall area, L^2, m^2
A_{SI}	impeller channel total wall area, L^2, m^2
C_1	absolute fluid velocity at impeller inlet, L/T, m/s
C_{1M}	meridional velocity at impeller inlet, L/T, m/s
C_{1U}	fluid tangential velocity at impeller inlet, L/T, m/s
C_2	absolute fluid velocity at impeller outlet, L/T, m/s
C_{2B}	absolute fluid velocity at impeller outlet corresponding to Q_{BM}, L/T, m/s
C_{2E}	effective velocity at impeller outlet, L/T, m/s
C_{2F}	fluid velocity outside impeller, L/T, m/s
C_{2M}	meridional velocity at impeller outlet, L/T, m/s
C_{2P}	projected velocity, L/T, m/s
C_{2U}	fluid tangential velocity at impeller outlet, L/T, m/s
C_D	drag coefficient

C_H	head correction factor
d	impeller diameter, L, m
D_C	representative impeller channel width at outlet, L, m
D_D	diffuser representative (hydraulic) diameter, L, m
D_I	impeller representative (hydraulic) diameter, L, m
D_L	leakage diameter, L, m
dP	differential pressure, M/(LT^2), Pa
f	friction factor
f_{FD}	friction factor in diffuser
f_{FI}	friction factor in impeller
f_{LK}	leakage friction factor
f_{TD}	local drag coefficient in diffuser
f_{TI}	local drag coefficient in impeller
F_γ	cross-section shape effect
F_β	pipe curvature effect
F_ω	rotational speed effect
h	channel height, L, m
H	pump head, L, m
H_{BEP}	head at BEP, L, m
H_E	Euler's Head, L, m
H_{EE}	effective Euler's Head, L, m
H_{FD}	head loss due to friction in diffuser, L, m

H_{FI}	head loss due to friction in impeller, L, m
H_{LK}	pressure head difference across leakage, L, m
H_{TD}	head loss due to turn in diffuser, L, m
H_{TI}	head loss due to turn in impeller, L, m
L_D	diffuser channel length, L, m
L_{LK}	leakage channel length, L, m
L_I	impeller channel length, L, m
N	rotational speed, 1/T, RPM
N_s	specific speed
P	pressure, M/(LT^2), Pa
P_2	shaft power, ML^2 /T^3 , kg·m^2 /s^3
P_{hyd}	hydraulic power, ML^2 /T^3 , kg·m^2 /s^3
Q	volumetric flow rate, L^3/T, m^3/s
q_{BEP}	flow rate at BEP, L^3/T, m^3/s
Q_{BM}	best match flow rate, L^3/T, m^3/s
Q_{LK}	leakage volumetric flow rate, L^3/T, m^3/s
R_1	radius of impeller inlet, L, m
R_2	radius of impeller outlet, L, m
Re	Reynolds number
Re_C	recirculation effect Reynolds number
Re_D	Reynolds numbers in diffuser
Re_I	Reynolds numbers in impeller

Re_L	leakage Reynolds number
R_{LK}	radius corresponding to leakage, L, m
S_L	leakage width, L, m
St	Strouhal number
t	time, T, s
T	temperature, ℃
T	blade thickness, L, m
U_1	impeller tangential velocity at inlet, L/T, m/s
U_2	impeller tangential velocity at outlet, L/T, m/s
U_{LK}	tangential velocity due to impeller rotation at leakage, L/T, m/s
v	velocity, L/T, m/s
V	volume, L^3, m^3
V_D	representative fluid velocity in diffuser, L/T, m/s
V_I	representative fluid velocity in impeller, L/T, m/s
V_L	fluid velocity at leakage, L/T, m/s
Vol_D	diffuser channel volume, L^3, m^3
Vol_I	impeller channel volume, L^3, m^3
V_S	shear velocity, L/T, m/s
W_1	relative velocity with respect to impeller at inlet, L/T, m/s
W_2	relative velocity with respect to impeller at outlet, L/T, m/s
We	Weber number
y_{I1}	impeller inlet height, L, m

y_{I2}	impeller outlet height, L, m
Z_I	impeller blade number

Greek Symbols

η	efficiency
μ	dynamic viscosity, M/(LT), Pa·s
μ_E	effective viscosity, M/(LT), Pa·s
μ_m	mixture viscosity, M/(LT), Pa·s
μ_o	oil viscosity, M/(LT), Pa·s
μ_w	water viscosity, M/(LT), Pa·s
μ_C	continuousviscosity, M/(LT), Pa·s
μ_A	model viscosity, M/(LT), Pa·s
β_1	blade angle from tangential at impeller inlet, °
β_2	blade angle from tangential at impeller outlet, °
v	kinematic viscosity, L^2/T, m^2/s
ρ	density, M/L^3, kg/m^3
σs	slip factor
ω	angular velocity, 1/T, 1/s
Ω	angular speed, L/T, m/s
φ	flow coefficient
ϕ	water fraction, %
ϕ_{max}	inversion point

ϕ_D	volume fraction of dispersed phase, %
ϕ_o	oil fraction, %
ϕ_w	water fraction, %
ψ	head coefficient

BIBLIOGRAPHY

1. Alboudwarej, H., Muhammad, M., Shahraki, A.K. et al. 2007. Rheology of Heavy-Oil Emulsions. *SPE Production & Operation*, 22 (3): 285–293. SPE-97886-PA.
2. Arirachakaran, S., Oglesby, K.D., Malinowsky, M.S. et al. 1989. An Analysis of Oil/Water Flow Phenomena in Horizontal Pipes. Paper presented at the SPE Production Operations Symposium, Oklahoma City, Oklahoma, USA, 13–14 March.
3. Banjar, H. and Zhang, H.-Q. 2019. Experiments and Emulsion Rheology Modeling in an Electric Submersible Pump. Paper presented at the International Petroleum Technology Conference, Beijing, China, 26–28 March. IPTC-19463-MS
4. Banjar, H.M. 2018. Experiments, CFD Simulation and Modeling of Oil Viscosity and Emulsion Effects on ESP Performance. Doctoral Dissertation, University of Tulsa, Tulsa, Oklahoma, USA.
5. Barrios, L., Rojas, M., Monteiro, G. et al. 2017. Brazil Field Experience of ESP Performance with Viscous Emulsions and High Gas Using Multi-Vane Pump MVP and High Power ESPs. Paper presented at the SPE Electric Submersible Pump Symposium, The Woodlands, Texas, USA, 24–28 April. SPE-185141-MS.
6. Barrios, L.J., Scott, S.L., Rivera, R., and Sheth, K.K., 2012. ESP Technology Maturation: Subsea Boosting System with High GOR and Viscous Fluid. Paper presented at the SPE Annual Technical Conference and Exhibition, San Antonio, Texas, USA, 8–10 October 2012. SPE-159186-MS.

7. Brinkman, H.C. 1952. The Viscosity of Concentrated Suspensions and Solutions. *J Chem Phys* 20 (4): 571–571.

8. Bulgarelli, N.A.V., Biazussi, J.L., Monte Verde, W. et al. 2020. Experimental Study of Phase Inversion Phenomena in Electrical Submersible Pumps under Oil/Water Flow. *J Offshore Mech Arct Eng*, 142 (4): 041402.

9. Churchill, S.W. 1977. Friction-Factor Equation Spans All Fluid-Flow Regimes. *Chem Eng*, 84 (24): 91–92.

10. Colebrook, C.F. 1939. Turbulent Flow in Pipes with Particular Reference to the Transition Region between the Smooth and Rough Pipe Laws. *Jour Inst Civil Eng (London)*, 11 (4): 133-156.

11. Croce, D., 2014. Study of Oil/Water Flow and Emulsion Formation in Electrical Submersible Pumps. MS Thesis, The University of Tulsa.

12. Croce, D.D. and Pereyra, E. 2020. Study of Oil/Water Flow and Emulsion Formation in Electrical Submersible Pumps. *SPE Production & Operation*, 35 (1): 26–36. SPE-198900-PA.

13. Einstein, A. 1911. Elementary Consideration of the Thermal Conductivity of Dielectric Solids. *Ann Phys German*, 34: 591.

14. Gamboa, J., and Prado, M., 2011. Review of Electrical-submersible-pump Surging Correlation and Models. *SPE Production & Operations*, 26(04): 314-324.

15. Gulich, J.F. 1999. Pumping Highly Viscous Fluids with Centrifugal Pumps-Part 1. *World Pumps*, 1999 (395): 30–34.

16. Khalil, M., Kassab, S., Ismail, A. et al. 2008. Centrifugal Pump Performance under Stable and Unstable Oil-Water Emulsions Flow. Paper presented at the 12th International Water Technology Conference, Alexandria, Egypt, 27–30 March.

17. Laflin, G.C. and Oglesby, K.D. 1976. An Experimental Study on the Effects of Flow Rate, Water Fraction and Gas Liquid Ratio on Air-Oil-Water Flow in Horizontal Pipes. B.Sc Thesis, University of Tulsa, Tulsa, Oklahoma, USA.

18. Morales, R., Pereyra, E., Wang, S. et al. 2013. Droplet Formation through Centrifugal Pumps for Oil-in-Water Dispersions. *SPE J*, 18 (1): 172–178. SPE-163055-PA.

19. Ofuchi, E.M., Stel, H., Vieira, T.S. et al. 2017. Study of the Effect of Viscosity on the Head and Flow Rate Degradation in Different Multistage Electric Submersible Pumps Using Dimensional Analysis. *J Pet Science Engineering*, 156: 442–450.

20. Peng, J. 2020. Experiments and Modeling of ESP Performance with Viscous Oils and Oil-Water Emulsions. Master Thesis, University of Tulsa, Tulsa, Oklahoma, USA.

21. Siddique, H.M., Chon, H.B., Samad, A. 2017. Effect of Crude Oil-Water Emulsions at Various Water-Cut on the Performance of the Centrifugal Pump. *Int. J. Oil, Gas and Coal Technology*, Vol. 16, No. 1, 2017

22. Solano, E.A. 2009. Viscous Effects on the Performance of Electro Submersible Pumps (ESP's). Master Thesis, University of Tulsa, Tulsa, Oklahoma, USA.

23. Sun, D. and Prado, M.G. 2006. Single-Phase Model for Electric Submersible Pump (ESP) Head Performance. *SPE J*, 11 (1): 80–88. SPE-80925-PA.

24. Takács, G., 2009. Electrical Submersible Pumps Manual: Design, Operations, and Maintenance. Gulf Professional Publishing, Burlington, USA.

25. Vielma, J.C. 2006. Rheological Behavior of Oil-Water Dispersion Flow in Horizontal Pipes. MS Thesis, University of Tulsa, Tulsa, Oklahoma, USA.

26. Vand, V. 1948. Viscosity of Solutions and Suspensions. I. Theory. *J Phys Chem*, 52 (2): 277–299.

27. Wiesner, F.J. 1967. A Review of Slip Factors for Centrifugal Impellers. *ASME J Eng Power*, 89 (4): 558–566.

28. White, F.M. 1998. Internal Versus External Viscous Flows. In Fluid Mechanics. Rhode Island: McGraw-Hill.

29. Wood Group ESP, 2004. Product Catalog. Wood Group ESP, Inc, Oklahoma City, OK.

30. Zande, V., Muntinga, J. and Broek, W. 1999. The effects of production rate and choke size on emulsion stability." EXPL-6-MZ, INGEPET '99.

31. Zhang, J. 2017. Experiments, CFD Simulation and Modeling of ESP Performance under Viscous Fluid Flow Condition. MS Thesis, The University of Tulsa.

32. Zhang, H. 2020. PE 7003 Artificial Lift System. Lecture Notes, The University of Tulsa.

33. Zhang, H.-Q., 2013-2018. Proceedings of TUALP Spring Advisory Board Meeting, the University of Tulsa, Tulsa, OK.

34. Zhu, J., Zhu, H., Cao, G. et al. 2019a. A New Mechanistic Model to Predict Boosting Pressure of Electrical Submersible Pumps under High-Viscosity. Fluid Flow with Validations by Experimental Data. Paper presented at the SPE Gulf Coast Section Electric Submersible Pumps Symposium, The Woodlands, Texas, USA, 13–17 May. SPE-194384-MS.

35. Zhu, J., Hattan Banjar, Zhenyan Xia, Hong-Quan Zhang 2016. CFD simulation and experimental study of oil viscosity effect on multi- stage electrical submersible pump (ESP) performance. *Journal of Petroleum Science and Engineering*, 146 (16): 735-745

36. Zhu, J., Zhu, H., Cao, G. Banjar, H. et al. 2019. A New Mechanistic Model for Oil-Water Emulsion Rheology and Boosting Pressure Prediction in Electrical Submersible Pumps ESP. Paper presented at the SPE Annual Technology Conference and Exhibition. Calgary, Alberta, Canada, 30 September – 2 October. SPE-196155-MS.

APPENDIX A

EXPERIMENTAL LOOP - EQUIPMENT AND INSTRUMENT SPECIFICATIONS

Table A.1 TUALP High-Viscosity ESP Flow Loop Equipment Specifications

Equipment	Model	Capacity	Purpose
ESP	GE Oil & Gas Wood Group TE-2700	BEP: 2700 bpd, 3500 RPM	Testing Bench
Electric Motor	North American H3650	50 hp	Drive Motor
Air Compressor	Kaeser CSD60	186 cfm, 217 psi	Air Source
Air Pressure Regulator	Speedaire 4ZM22	300 psi Max Inlet Pressure, 150 psi Max Outlet Pressure	Air Pressure Regulation
Variable Speed Drive	Hitachi L300P	50 hp	Altering Rotational Speed
ESP Thrust Chamber	Schlumberger REDA NO.88AB1- LT	-	Thrust Bearing Box
Liquid Pneumatic Control Valve	Fisher Body EDActuator 657 Positioner 582i	-	Liquid Flow Rate Control
Water Pump	Dayton Stainless SteelCentrifugal Pump 2ZWT9A	0.5 hp	Water Circulation
Water Tank	Value Brand T-0300-059	300 gal	Water Storage
Water Pneumatic Control Valve	Fisher Body V100Actuator 1052 Positioner 3622	-	Water Flow Rate Control

Table A.2 TUALP High-Viscosity ESP Flow Loop Instrumentation Specifications

Instrument	Model	Range	Accuracy
Thermocouple	Thermo Electric TCMSC83077875	0 to 1600 °F	±0.75%
Resistance Temperature Detector	Omega PR-11-2-100-1/8-18-E	-200 to 600 °C	±0.15°C
Temperature Transmitter	INOR IPAQ R520	-	-
Absolute Pressure Transmitter	Emerson Rosemount 2051	0 to 500 psi	±0.1%
Differential Pressure Transmitter	Emerson Rosemount 3051S	-10 to 50 psig	±0.1%
Pipe Viscometer	Emerson Rosemount 3051S	-250 to 250 psig	±0.1%
Coriolis High Flow Rate Meter	Proline Promass 80E	0 to 6615 lb/min	Mass Flow: ±0.2% Volume Flow: ±0.2% Density: ±0.0005 g/cm^3
Coriolis Low Flow Rate Meter	Micro Motion CMF200	0 to 1600 lb/min	Mass Flow: ±0.1% Volume Flow: ±0.1% Density: ±0.0005 g/cm^3

Table A.3 TUALP High-Viscosity ESP Flow Loop DAQ Specifications

Device	Features
Data Processing Computer	Dell Optiplex 9020, i7-4770 CPU @ 3.4 GHz, RAM: 16GB, HD: 1TB
National Instruments cFP-AI-110	• Eight analog voltage or current input channels • Eight voltage input ranges: 0–1 V, 0–5 V, 0–10 V, ±60 mV, ±300 mV, ±1 V, ±5 V, and ±10 V • Three current input ranges: 0–20, 4–20, and ±20 mA • 16-bit resolution • Three filter settings: 50, 60, and 500 Hz • 250 V_{rms} CAT II continuous channel-to-ground isolation, verified by 2,300 V_{rms} dielectric withstand test • –40 to 70 °C operation • Hot-swappable
National Instruments cFP-AI-111	• Sixteen single-ended analog current input channels • Three input ranges: ±20, 0–20, and 4–20 mA • 16-bit resolution • Three filter settings: 50, 60, and 500 Hz • Hot-swappable

	• 2300 V_{rms} transient overvoltage protection • –40 to 70 °C operation
National Instruments cFP-AO-200	• Eight 0–20 or 4–20 mA outputs • 0.5 mA over ranging • 12-bit resolution • Up to 1 kΩ load impedance (with 24 V loop supply) • Indicators for open current loops • Short-circuit protection • 2300 V_{rms} transient overvoltage protection between the inter-module communication bus and the I/O channels • –40 to 70 °C operation Hot plug-and-play
National InstrumentscFP-1804	• Network interface: 10 BaseT and 100 BaseTX Ethernet, IEEE802.3, 10/100 Mbps • One RS-232 (DCE) serial port, 300 to 115200 bps • 11 to 30 VDC, 20W • 2300 V_{rms} transient overvoltage protection • –40 to 70 °C operation
National InstrumentscFP-CB-1	• cFP-CB-1 is designed for general-purpose and hazardous voltage1 operation with all Compact FieldPoint I/O modules • 36 terminals available • Tie-wrap anchors for wires • Color-coded V and C terminals for voltage supply and common connections • –40 to 70 °C operation

Table A.4 Coriolis Flow Meters Specifications

	High Flow Meter	**Low Flow Meter**
Model	Promass 80E	CMF200M
Brand	Endress+Hauser	Emerson
Meter Size (inch)	3	2
Accuracy	0.20%	0.25%
Accurate Measurement Range (bpd)	>1700	>150
Pressure Drop at 300 cp (psi)	12.2 at 10,000 bpd	13.7 at 2,100 bpd
Pressure Drop at 700 cp (psi)	18.8 at 10,000 bpd	25.6 at 2,100 bpd
Pressure Drop at 1000 cp (psi)	23.0 at 10,000 bpd	34.1 at 2,100 bpd

Table A.5 Pipe-in-Pipe Heat Exchanger Design Data

	Fluid
Heat Transfer Media	Water
Volume Flow Rate (bpd)	1940
Inlet Temperature (°C)	0
Outlet Temperature (°C)	1
Density (kg/m^3)	1001
Specific Heat (W/K)	4129
Viscosity (cp)	1.7
Thermal Conductivity (W/m·K)	0.570
Pressure Drop (psi)	0.00
Log Mean Temp Difference (°C)	34.25
Heat Transfer Rate (BTU/hr)	50375
Heat Transfer Area (ft^2)	21
Length (ft)	27

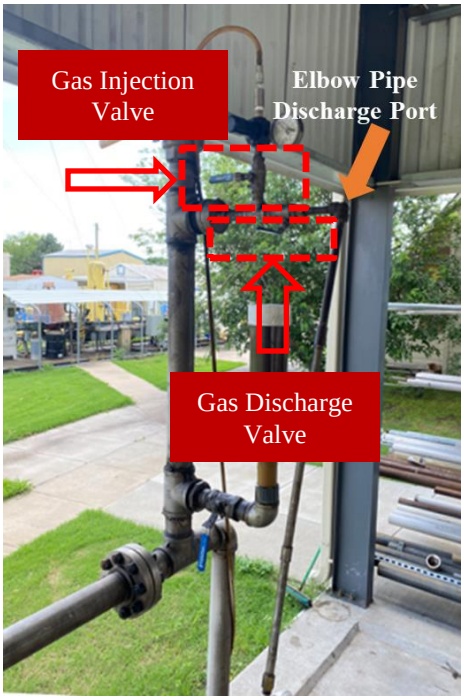

Figure A.1 Pressurization Port and Gas Discharge Valve

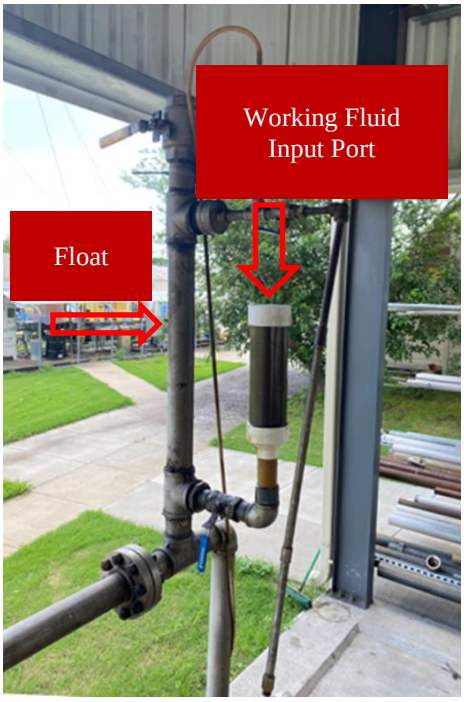

Figure A.2 Working Fluid Injection Port

Figure A.3 Coriolis Flow Meter

Figure A.4 Temperature Sensor

Figure A.5 Temperature Sensor

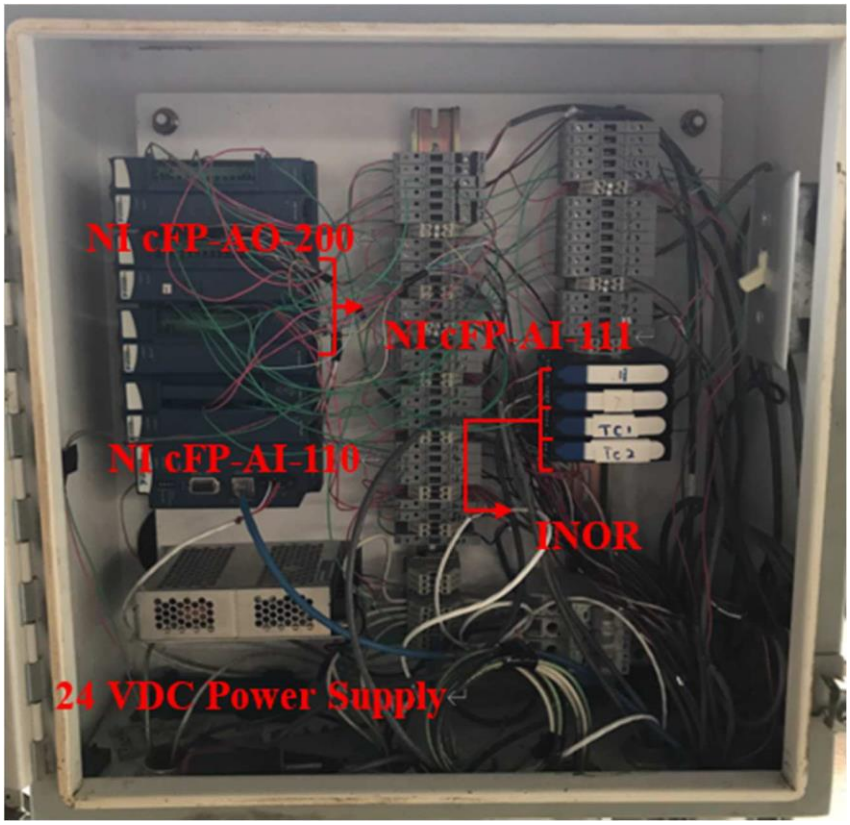

Figure A.6 Data Acquisition Modules

Figure A.7 Pressure Monitors

Figure A.8 Pneumatic Control Valve

Figure A.9 Cooling System

Figure A.10 Pipe-in-Pipe Heat Exchanger

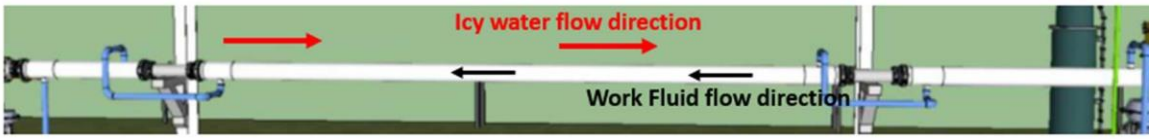

Figure A.11 Fluid Flow Schematic inside the Heat Exchanger

Figure A.12 Rotational Viscometer

Figure A.13 Water bath Temperature Control and Circulator

APPENDIX B

DIMENSIONLESS ANALYSIS

Emulsion rheology modeling in a highly shearing flow field is very challenging. Emulsion rheology is affected by many factors, including density, volumetric flow, stage diameter, viscosity, the interfacial tension, and pump rotational speed. Dimensional analysis was performed with Buckingham Pi Theorem for the emulsion rheology model. The table below shows the basic dimensions for each parameter:

Table B.1 Dimensional Analysis Variables

Variables	**ρ**	**Q**	**D**	**μ**	**σ**	***f***
Basic dimensions	$\frac{M}{L^3}$	$\frac{L^3}{T}$	L	$\frac{M}{L\,T}$	$\frac{M}{T^2}$	$\frac{1}{T}$

From Table B.1 there are 6 variables with 3 basic dimensions *M*, *L* and *T*, and thus 3 dimensionless groups are derived. By selecting the first 3 variables (**ρ**, **Q**, and **D)** as the repeated variables in each group, we have

$$\pi_1 = \rho[\frac{M}{L^3}]^a\ Q[\frac{L^3}{T}]^b\ D[L]^c\ \mu[\frac{M}{L.T}] = M^0L^0T^0, \quad \text{(B.1)}$$

$$\pi_2 = \rho[\frac{M}{L^3}]^a\ Q[\frac{L^3}{T}]^b\ D[L]^c\ \sigma[\frac{M}{T^2}] = M^0L^0T^0, \quad \text{(B.2)}$$

and

$$\pi_3 = \rho[\frac{M}{L^3}]^a\ Q[\frac{L^3}{T}]^b\ D[L]^c\ f[\frac{1}{T}] = M^0L^0T^0. \quad \text{(B.3)}$$

Solving for the exponents a, b, and c for equation (B.1), (B.2) and (B.3). And the results are: π_1:

a=-1, b=-1 and c=1, π_2: a=-1, b=-2 and c=3, π_3: a=0, b=-1 and c=3. Substituting these exponents to the equations and yields

$$\pi_1 = \frac{D\,\mu}{\rho\,Q} = \frac{D\,\mu}{\rho\,v\,A} = \frac{D\,\mu}{\rho\,v\,D^2} = \frac{\mu}{\rho\,v\,D} = \frac{1}{Re}, \quad \text{(B.4)}$$

$$\pi_2 = \frac{D^3\sigma}{\rho\,Q^2} = \frac{V\,\sigma}{\rho\,Q^2} = \frac{V\,\sigma}{\rho\,v^2\,A^2} \cong \frac{\sigma}{\rho\,v^2\,l} = \frac{1}{We}, \quad \text{(B.5)}$$

and

$$\pi_3 = \frac{D^3 f}{Q} = \frac{V\,f}{Q} \cong \frac{l\,A\,f}{v\,A} = \frac{l\,f}{v} = St. \quad \text{(B.6)}$$

Other factors affecting the emulsion rheology cannot be derived with this analysis since they are already dimensionless, such as the fraction of the dispersed phase and the stage number.

APPENDIX C

THE STATISTICAL DEFINITIONS OF ERRORS

Statistical definitions of errors are used to demonstrate the performance of the mechanistic model by comparing the model predicted ESP boosting pressure against the corresponding experimental data (Wang et al. 2014). Two categories of errors, namely the actual error and the relative error, are defined. Based on the relative error and actual error, six statistical parameters are defined: average relative error (ε_1), absolute average relative error (ε_2), standard deviation of relative error (ε_3), average actual error (ε_4) absolute average actual error (ε_5), and standard deviation of actual error (ε_6). The calculation of statistical parameters is presented below:

- The average relative error,

$$\varepsilon_1 = \frac{1}{N}\sum_{I=1}^{N} e_{i.} \quad \text{(D.1)}$$

- The absolute average relative error,

$$\varepsilon_2 = \frac{1}{N}\sum_{I=1}^{N} |e_i|. \quad \text{(D.2)}$$

- The standard deviation of relative error,

$$\varepsilon_3 = \sqrt{\frac{\sum_{I=1}^{N}(e_i - \varepsilon_1)^2}{N-1}}. \quad \text{(D.3)}$$

- The average actual error,

$$\varepsilon_4 = \frac{1}{N}\sum_{I=1}^{N} e_j. \quad \text{(D.4)}$$

- The absolute average actual error,

$$\varepsilon_5 = \frac{1}{N}\sum_{I=1}^{N}\left|e_j\right|. \quad \text{(D.5)}$$

- The standard deviation of actual error (ε_6):

$$\varepsilon_6 = \sqrt{\frac{\sum_{I=1}^{N}(e_j - \varepsilon_4)^2}{N-1}}. \quad \text{(D.6)}$$